NASA Contractor Report 177568

A Novel Potential/Viscous Flow Coupling Technique for Computing Helicopter Flow Fields

J. Michael Summa, Daniel J. Strash, and Sungyul Yoo

CONTRACT NAS2-12962
August 1990

National Aeronautics and Space Administration

NASA Contractor Report 177568

A Novel Potential/Viscous Flow Coupling Technique for Computing Helicopter Flow Fields

J. Michael Summa
Daniel J. Strash
Sungyul Yoo
Analytical Methods, Inc.
Redmond, Washington

Prepared for
Ames Research Center
CONTRACT NAS2-12962
August 1990

National Aeronautics and
Space Administration

Ames Research Center
Moffett Field, California 94035-1000

TABLE OF CONTENTS

SUMMARY

Because of the complexity of the helicopter flow field, a zonal method of analysis of computational aerodynamics is required. The objective of this research is to demonstrate the feasibility of a new potential/viscous coupling procedure for reducing computational effort while maintaining solution accuracy.

A closed-loop overlapping velocity-coupling procedure has been developed with the unique feature that the potential flow singularity strengths are obtained from the Navier-Stokes solution at an inner fluid boundary. This procedure has been utilized to combine a two-dimensional potential flow code and a two-dimensional Navier-Stokes code, ARC2D, developed by Pulliam and Steger at NASA Ames.

The resultant fully coupled code, ZAP2D (Zonal Aerodynamics Program-2D), has been used to compute the flow past a NACA 0012 airfoil. For this case the zonal method has shown that the grid domain size can be reduced to 0.25 chord lengths with no loss in accuracy. The numerical behavior of the ARC2D solution is also greatly improved due to the reduced domain size. Finally, the computation time is reduced by approximately a factor of 10 for given accuracy.

Additional reductions in domain size and accelerated convergence methods should decrease the required ZAP2D computation time to about a factor of 20 compared with the ARC2D simulation. This level of computational speed achievable with ZAP2D would allow for the development of a fully interactive program that could be used for preliminary airfoil design. More importantly, perhaps, similar grid density reductions in three dimensions would result in significant decreases in memory requirements and potential computation time reductions for such a zonal approach of at least one order of magnitude.

This improvement in computational effort should then provide the means for more accurate viscous and compressible simulations of the complex flow fields associated with rotary wing aircraft and should translate into improved analysis of such important performance parameters as helicopter fuselage drag and rotor airloads.

1.0 INTRODUCTION

The flow fields associated with rotary wing aircraft, including the tilt-rotor helicopter, are extremely complicated and remain a challenge for applied computational aerodynamics. While linear methods or pure potential flow models of nonlinear wake shape effects have become commonly used techniques for helicopter aerodynamics predictions and analyses, the nonlinear methods that incorporate more correct mathematical models of the actual flow physics--such as compressibility and viscosity--are being developed and applied by research scientists. Much progress has been made in solving the full potential, Euler, and various forms of the approximate Navier-Stokes equations; however, because of the wide variation of physical scales of characteristic fluid phenomena from boundary layer thickness and vortex core radius to rotor diameter, a zonal method of analysis is generally projected for the entire helicopter flowfield calculation. This is necessary not only to achieve a closed calculation on the next generation of computers, but also to obtain the required numerical accuracy over such large regions that must include fine meshes to resolve the viscous layers as well as large flow gradients. Consequently, full closed-loop coupling methods need to be developed for these zonal calculations.

In the Phase I work described in this report, a new general procedure for coupling potential and viscous flow calculation schemes has been developed and demonstrated for a two-dimensional airfoil simulation. The coupling method is based on the premise that any computational method can only produce valid results within the approximations of the physical model employed in its construction. Therefore, the interfacing boundary surface between the potential and viscous flow code domains must be very nearly potential in order to achieve a successful (accurate) result. Specifically, during Phase I, an AMI (Analytical Methods, Inc.) two-dimensional, potential flow panel method, program POT2D, has been coupled with a NASA Ames two-dimensional, thin-layer, Navier-Stokes code, ARC2D (1). An overlapping velocity coupling procedure is utilized with the unique feature that (beyond the first iteration) the potential flow surface panel strengths (ϕ and $\partial\phi/\partial n$) are obtained directly from the Navier-Stokes solution at a smooth inner fluid boundary. These fluid surface panel values are then used to compute the outer velocity boundary conditions for the Navier-Stokes calculation. The iteration between the potential flow solution and the Navier-Stokes solution continues in a closed loop until flow convergence or allowable iteration limits are obtained. The resultant fully coupled code is called ZAP2D for Zonal Aerodynamics Program (2D).

The primary objective of the current work is then to demonstrate the feasibility of the coupling procedure installed in ZAP2D for reducing the computational effort, i.e., grid, required by ARC2D for a given accuracy. In the following sections the methodology required for the coupled program is first described briefly and then the detailed analysis of the zonal simulation of the flow past an airfoil is compared with the Navier-Stokes alone simulation as well as with experimental data.

2.0 METHODOLOGY

2.1 Zonal Method--ZAP2D

A new two-dimensional CFD method, ZAP2D (Zonal Aerodynamics Program), has been developed that combines potential and viscous flow calculation schemes. The actual coupling between the methods is based on the premise that the coupling boundary should be located in the computed flow field where the approximations inherent in both methods are valid; consequently, the interfacing boundary surface between the potential and viscous flow regions must be very nearly potential in order to achieve an accurate result.

The general coupling concept for the zonal method is illustrated in Figures 1 and 2. Figure 1 shows the zonal representation of the physical flow field while the flow chart of the iteration scheme is shown in Figure 2. An inner boundary, S_i, which is measured by a radius, say, R_i, is constructed to enclose a generally shaped body or airfoil and the fluid region near the body where viscous effects dominate. Although the body might be a complex shape, the inner boundary surface, S_i, would be a simple, smooth geometry. An additional outer surface, S_o, which is measured by a radius, say, R_o, also of simple shape, forms the computational domain of the viscous calculation. Of course, the potential flow is solved by the panel method beyond S_o to an infinite distance from the body surface.

The iterative coupling of the proposed method proceeds as follows (see Figure 2).

1. The calculation procedure is initialized by computing the potential flow associated with the body motion. An integral panel method is used for this computation. In this first step only the actual body surface is represented by discrete panels and the surface potential equation is solved directly by enforcing the Neumann boundary condition.

2. The velocity field, $\mathbf{V}_o$, on the outer boundary, S_o, is computed from the known potential flow surface singularity solution.

3. This velocity field, $\mathbf{V}_o$, serves as the outer boundary values for the Navier-Stokes calculation. Once the Navier-Stokes solution for the flow inside S_o is obtained, the velocity field due to the viscous solution, say $\mathbf{V}_i$ on S_i, which is just outside the region of viscous effects, is also known.

4. This inner boundary velocity, $\mathbf{V}_i$, can therefore be used to generate the known corresponding values of the velocity potential, ϕ, and its normal derivative to S_i, $(\partial\phi/\partial n)$. These represent the panel doublet and source strengths on S_i required for a new potential flow calculation; consequently, all further potential flow calculations require only the paneling of the smooth inner boundary, S_i, and not the actual body surface. Therefore, further calculations by the panel method of the outer boundary velocity field, $\mathbf{V}_o$, should be very accurate and any possible contamination of the Navier-Stokes simulation by potential flow numerical errors is minimized.

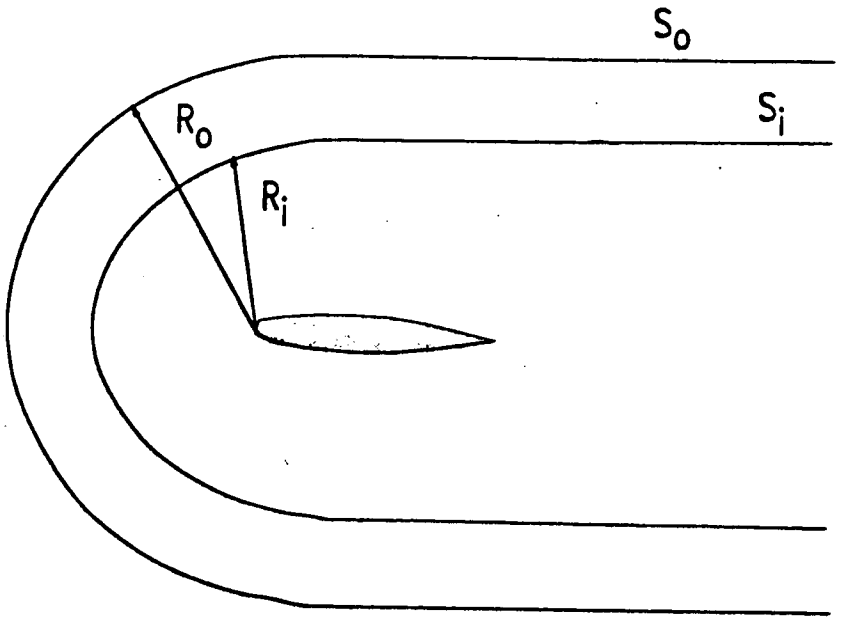

Figure 1. Zonal Representation of the Physical Flow Field.

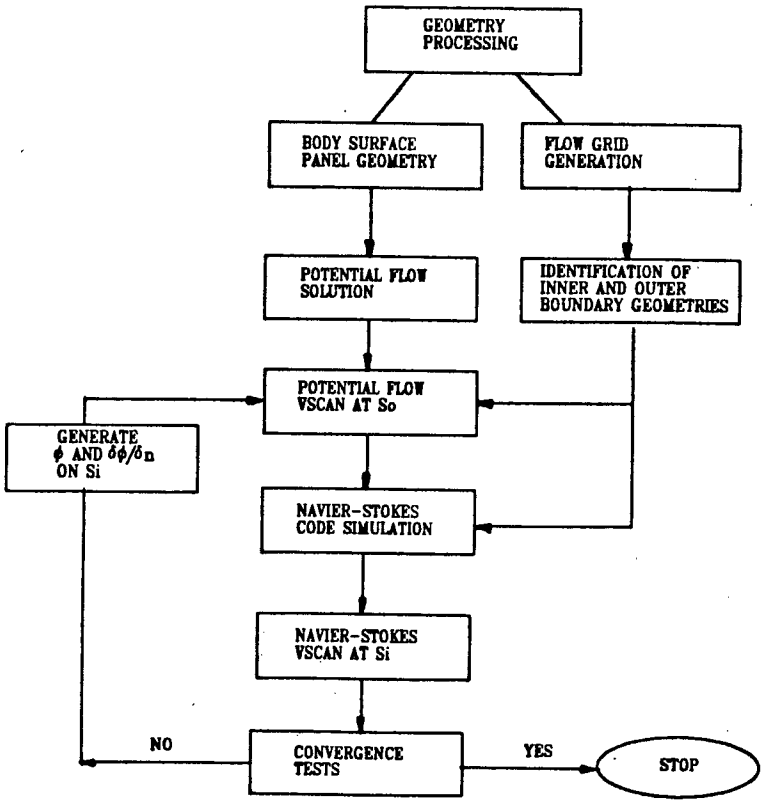

Figure 2. Flow Chart of the Zonal Iteration Scheme.

5. This iteration loop, Steps 2-4, is repeated until the inner boundary velocity, $\mathbf{V}_i$, is converged as measured by converged integrated forces and moments.

In order to validate such a coupling procedure it is important to select robust and computationally accurate potential and viscous simulation methods. POT2D was selected as the potential flow module since it was developed by AMI and formed the basis of the three-dimensional code, VSAERO (2), which has been widely used and validated. ARC2D was selected for the viscous flow module for much the same reasons--it is very widely used in the computation of airfoil aerodynamics and has also been extended to the three-dimensional case, ARC3D.

These two codes, POT2D and ARC2D, are briefly described below with emphasis given to the code modifications and accuracy testing required to accomplish the coupling procedure. In particular, the validity of the potential flow simulation for the open inner boundary, S_i, is of importance and is described in some detail.

2.2 Potential Flow Method--POT2D

As is well known, the potential describing an inviscid, irrotational, incompressible flow can be expressed by its boundary values (3). Specifically, an integral solution of Laplace's equation for the velocity potential can be derived by application of Green's theorem. The resultant boundary integral equation for the surface velocity potential is composed of two integrals:

1. a body surface integral of a doublet kernel function of strength, ϕ, and a source kernel function of strength, $\partial\phi/\partial n$, and

2. a thin wake surface integral of a doublet kernel function of strength, $\Delta\phi_w$.

Of course, the wake strengths, $\Delta\phi_w$, are related to the body surface potential, ϕ, through the wake auxiliary Kutta condition and the body source strengths, $\partial\phi/\partial n$, are known by the tangent flow boundary condition on the body. Hence the integral equation for ϕ can be solved directly as suggested by Morino (4). In POT2D, the integral equation is discretized and transformed to an algebraic equation by representing the boundaries with flat panels and approximating the local panel source and doublet strengths with constant values just as in VSAERO.

Once the surface potential is computed, surface velocities are obtained by numerical differentiation and forces and moments are found by pressure integration. Further, off-body flow velocities are computed by integration of surface velocity source and doublet influence functions. Finally, in the current code, the Karman-Tsien compressibility correction (5) based upon free stream Mach number and local velocity magnitude can also be utilized.

In the continued development of POT2D for the zonal method, surface solution accuracy, off-body velocity scan accuracy, and the accurate simulation of the open surface required for the inner boundary coupling were carefully analyzed. A summary of the specific test cases used and their implications are presented in Table 1. The results of each of these cases are discussed briefly below.

In case 1, the accuracy of the POT2D algorithm was tested by comparison with the exact solution for a circular cylinder with a dimensionless circulation equal to approximately 2.2. As shown in Figure 3, the comparison of the computed and exact surface pressure coefficient is remarkably accurate for a panel model consisting of only 80 upper surface elements. The computed off-body velocity magnitude is compared to the exact solution in Figure 4. The closest field velocity calculation is located approximately 10% of a diameter (or chord length) away from the cylinder surface. This distance would represent a typical minimum location for the inner boundary coupling surface. In this calculation, the panel number was also increased to 240 equally spaced panels in order to simulate the relative ratio of R_i to the maximum local panel size that would be expected for the airfoil calculations. As indicated in Figure 4, the maximum deviation in velocity magnitude from exact value at this location is on the order of one percent, which should be suitable for the zonal method.

A final example of the accuracy of POT2D for simulating the flow past a closed surface is shown in Figure 5. Here, the computed and experimental (6) surface pressures are compared for the NACA 0012 airfoil at 4.966 degrees angle of attack (Case 2). As expected, the potential flow solution from POT2D is very accurate over most of the airfoil, with the exception of areas near the leading and trailing edges, where viscous effects are important.

Since the POT2D simulation at the fluid inner boundary coupling surface, S_i, is driven by the ARC2D solution which is computed only a finite distance downstream, the potential flow simulation on this open surface must be extended to infinity. A wake model which implies a branch cut to infinity was installed in POT2D which cancels the vortex left at the upper and lower trailing edges due to the truncation of the potential doublet panels. A simple Rankine oval was utilized to verify the technique (Case 3). As presented in Figure 6, the deviation from the exact surface pressure coefficient is negligible over the entire surface and, in fact, is only evident as the trailing edge of the body is approached. This small error near the open end has recently been found to be due to the truncation of the perturbation source strength at the rear of the surface. While the influence of a linear source panel has been derived and added to the code to carry the source strength off onto the wake in order to recover free-stream conditions, this contribution has not been properly verified. Consequently, in all calculations presented here, this term is neglected, and the accuracy demonstrated here is assumed adequate for the proof-of-concept. Still, future improvements should include the proper decay of the surface source term to ensure an accurate solution which would be independent of the location of the inner boundary.

CASE	DESCRIPTION	PURPOSE	DATA CORRELATION		ALPHA	MACH NO.	RESULTS IN FIG. NO.
			EXACT OR NUMERICAL	EXP.			
1	2-D flow about a circular cylinder with circulation (Γ/V_∞/CHORD=2.2)	Test basic POT2D potential flow algorithm	X		0.0	0.0	3
		Examine accuracy of velocity field calculation in presence of a closed surface	X		0.0	0.0	4
2	2-D flow about a NACA 0012 airfoil	Examine accuracy of POT2D potential flow calculation as compared to experiment		X	4.966	0.3	5
3	2-D flow about a Rankine body (source and uniform flow)	Test open-surface wake extension	X		0.0	0.0	6
4	2-D flow about a NACA 0012 and its equivalent inner boundary model	Test ZAP2D coupling mechanics and field velocity calculation for both open and closed surfaces	X		5.0	0.0	7(a), (b) 8(a), (b)

Table 1. Summary of Test Cases used in the Potential Flow Validation.

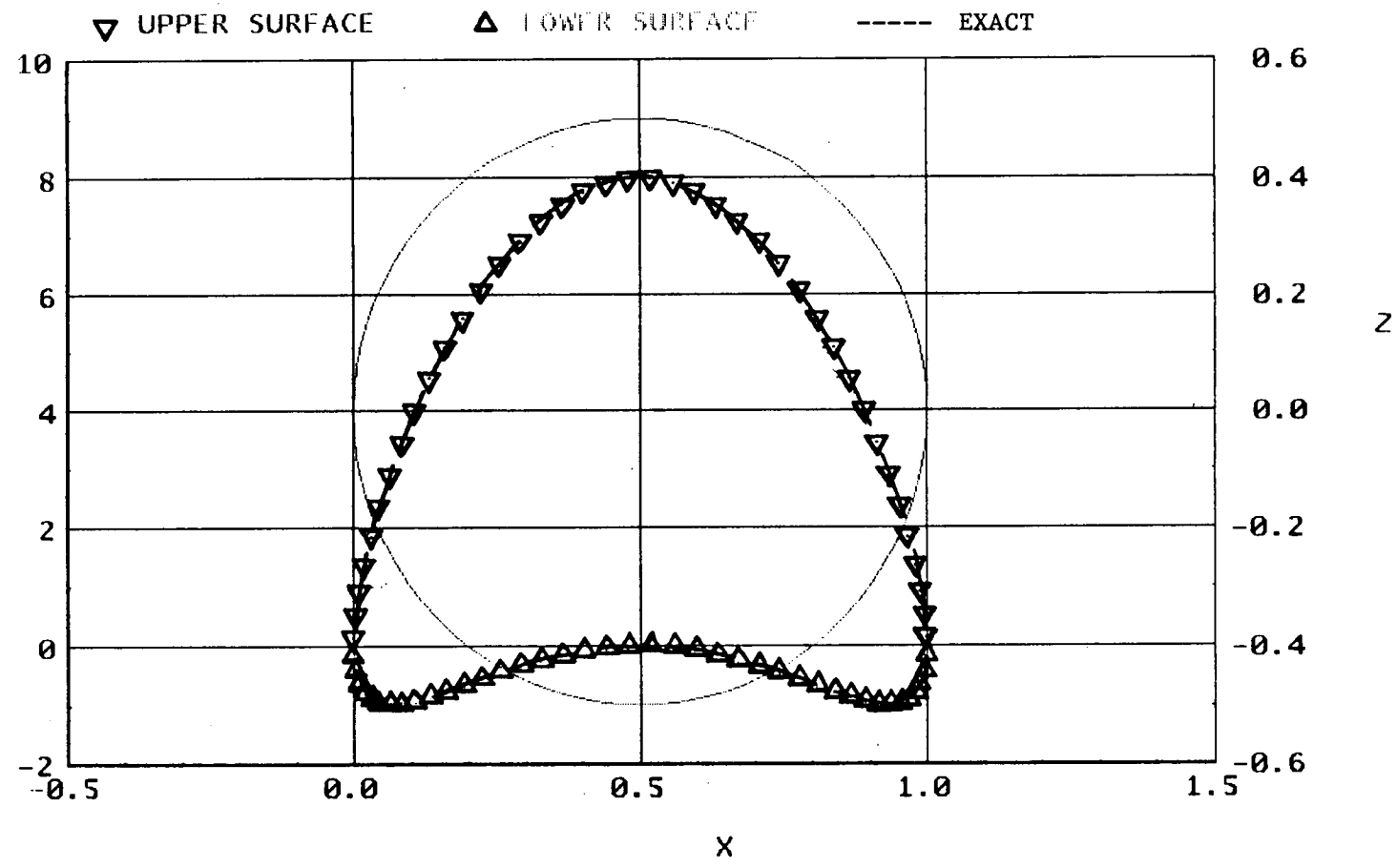

Figure 3. Comparison of Calculated and Exact Potential Flow Cp Distribution for a Two-Dimensional, Circular Cylinder with Circulation (Case 1, Table 1).

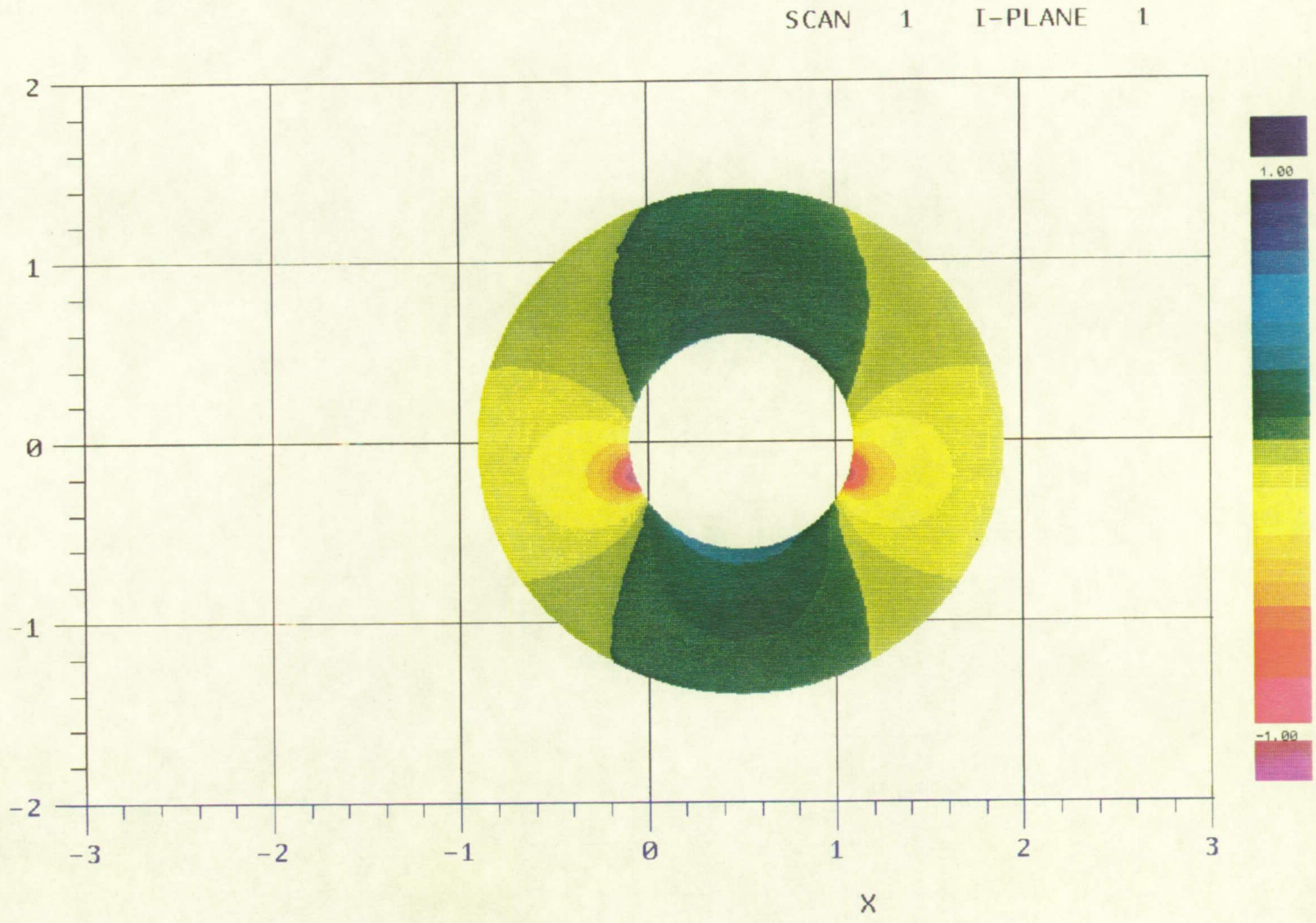

Figure 4. Calculated Field Velocity Error (%) from the Exact Potential Flow Solution for Two-Dimensional Circular Cylinder (Case 1, Table 1).

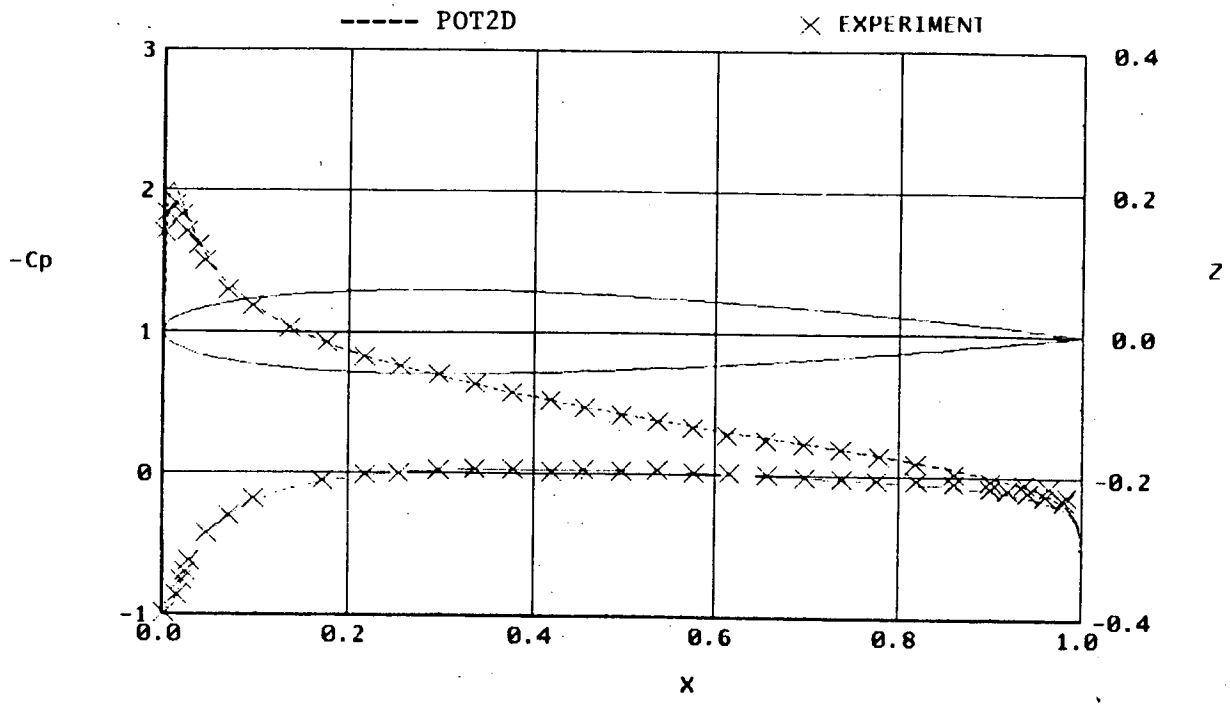

Figure 5. Comparison of Calculated and Experimental Cp Distribution for a NACA 0012 Airfoil at Mach 0.3, Alpha 4.966° (Case 2, Table 1).

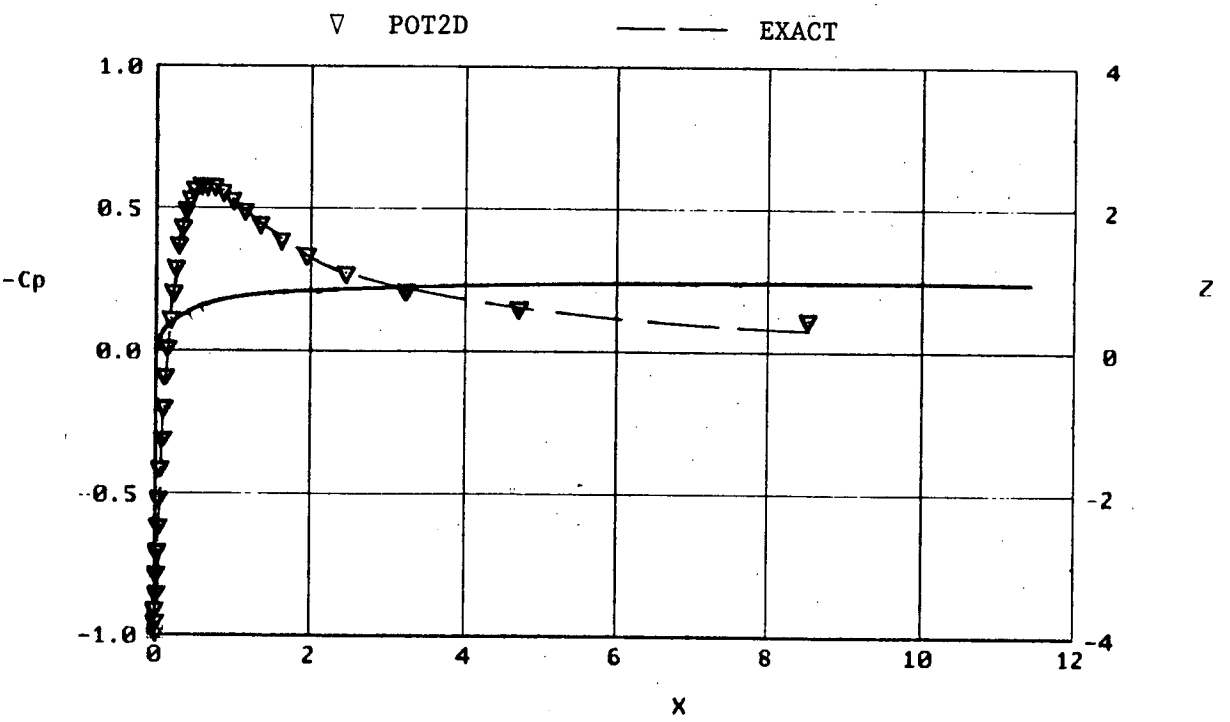

Figure 6. Comparison of Calculated and Exact Potential Flow Solution of Cp Distribution for Rankine Body (Case 3, Table 1).

To verify the mechanics of the ZAP2D coupling procedure, a rather interesting test case was devised (Case 4) . This case involved a pseudo-coupling procedure which was purely potential flow in nature. The initial part of this case involved the surface solution for the NACA 0012 airfoil at 5° angle of attack and a field velocity computation on a surface much like the inner boundary (S_i) shown in Figure 1. The field velocity components were combined to form the normal gradient in potential and used as boundary conditions for the second part of the validation case. This "inner boundary" solution, complete with $\partial\phi/\partial n$ specification, onset flow, and simple wake extension was then compared to the initial field velocity calculation in terms of the velocity components. As demonstrated by Figures 7(a) and (b), the part two inner boundary solution compares extremely well with the initial field solution for both V_x and V_z, respectively. The minor deviations near the peak velocities and near the wake region may be explained by the finite representation of the airfoil surface as this relates to the field velocity computation and the premature truncation of the trailing-edge source term previously mentioned.

The comparison between the field velocity calculation in the presence of the closed surface of part one (ITER=0) and the open surface (ITER=1) of part two is presented in Figures 8(a) and (b) for the two components of velocity. As indicated, the field velocity calculation generates nearly identical results regardless of whether the surface is open or closed.

As demonstrated by this battery of test cases, the accuracy of the potential flow solution generated by POT2D for both closed and open surfaces should minimize any induced numerical errors in the ARC2D boundary conditions.

2.3 Navier-Stokes Method--ARC2D

As noted earlier, ARC2D, originally developed by Pulliam and Steger (1) at NASA Ames, has been widely used in the computation of airfoil aerodynamics. The code has been continually improved by Pulliam and colleagues (7), (8) and (9), and the details of the theory are well documented in these references. Even though this code is written based on the "thin layer Navier-Stokes approximation" it is known to be adequate for separation problems with subsonic or transonic free streams when the flow field associated with separation is convection-dominated.

For turbulent flows, the well-known Baldwin-Lomax algebraic model (10) is used for turbulence closure. This turbulence model has been used in computing solutions for a wide variety of flow conditions and has been found to be acceptably accurate.

The numerical algorithm is an implicit approximate factorization finite difference scheme which can be either first- or second-order accurate in time.

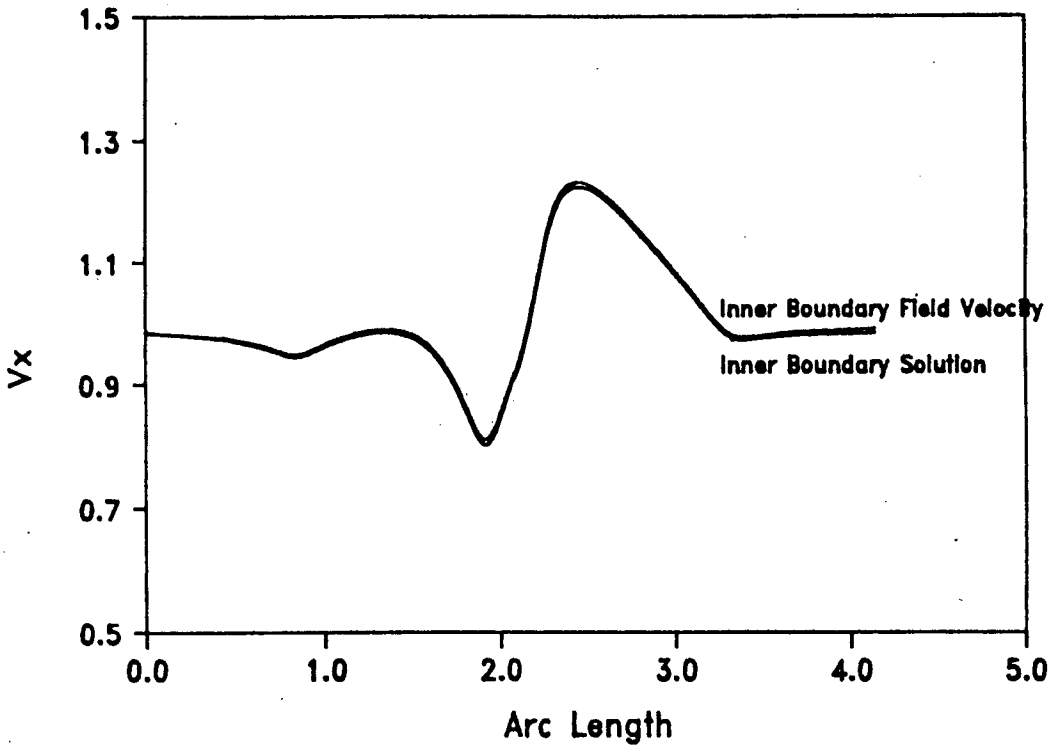

(a) Streamwise Components

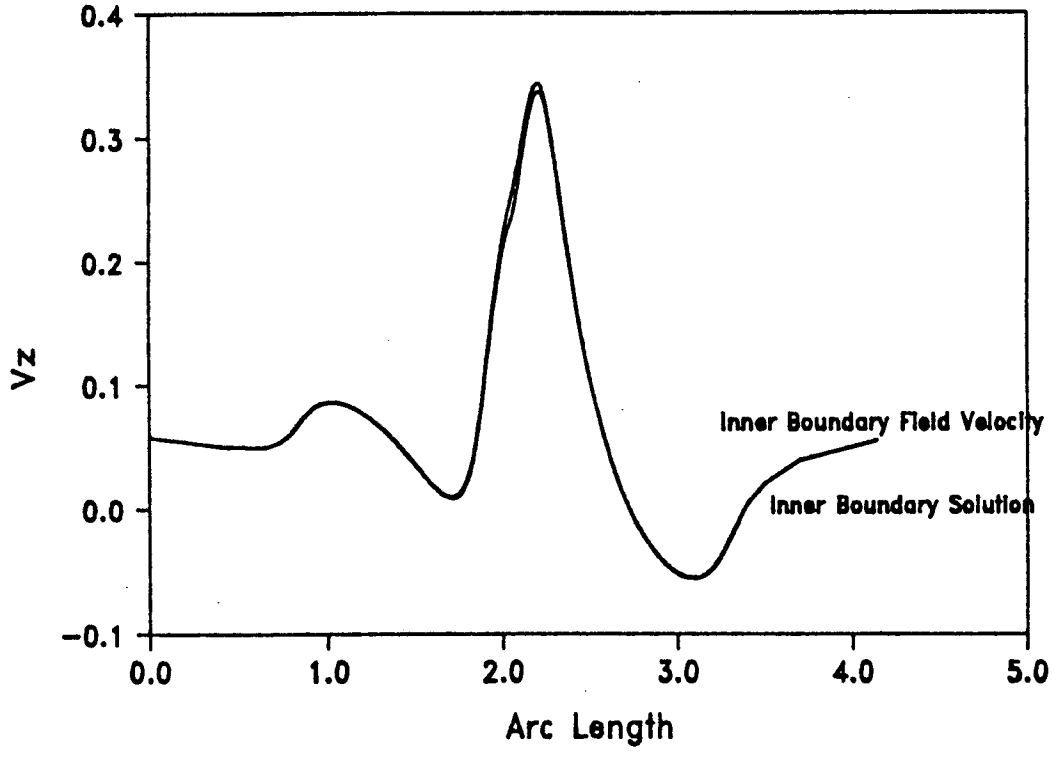

(b) Vertical Components

Figure 7. Comparison of Velocity Components for the Field Calculation and the "Equivalent" Surface Solution (Case 4, Table 1).

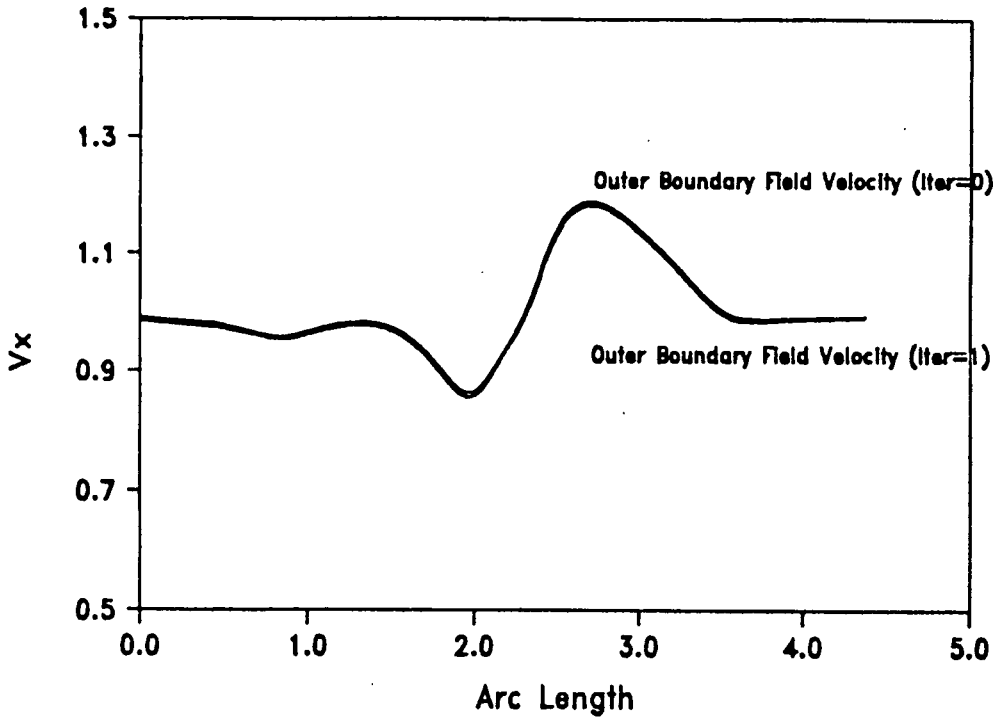

(a) Streamwise Components

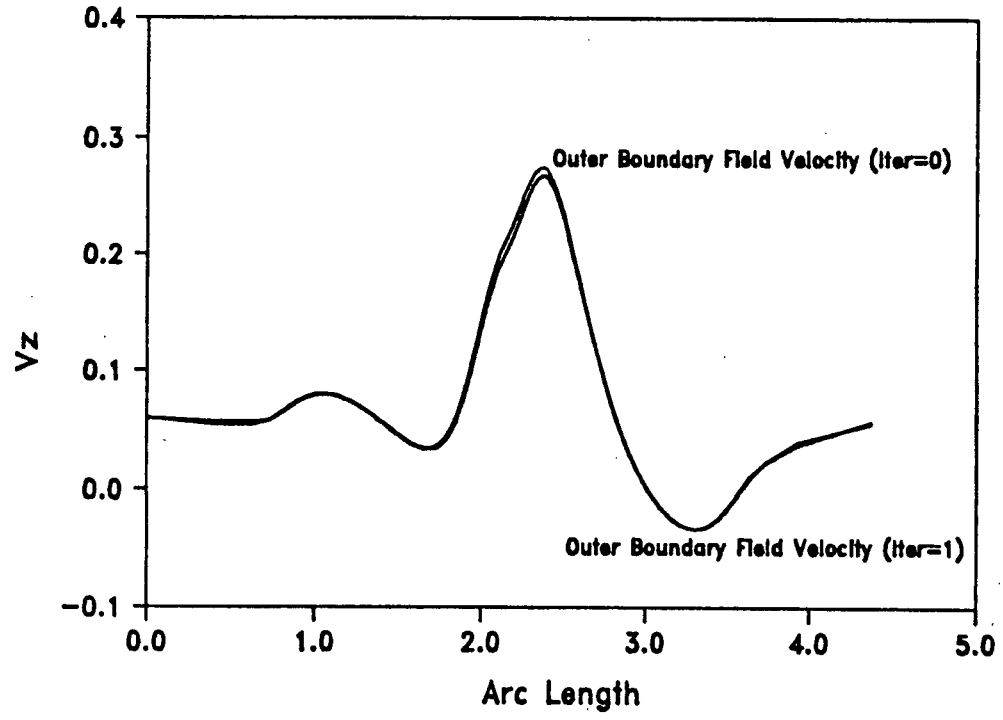

(b) Vertical Components

Figure 8. Comparison of Velocity Components for the Field Velocity Calculation on the Outer Boundary in the Presence of Both the Airfoil (ITER=0) and the "Equivalent" Surface (ITER=1).

Over the years of development of ARC2D, unique features have been added to the code to improve its capability to accurately predict aerodynamic characteristics for airfoil calculations.

One of these features is a far-field boundary treatment using the Riemann invariants concept and the other is an implementation of a simple viscous-inviscid coupling. In the far-field boundary condition, the outer boundary velocities are determined as a function of both the outer boundary velocities and the velocities extrapolated from the inner points. In this calculation the normal velocity component at the boundary is determined as an average of the Riemann invariants. The tangential velocity component is obtained from either the outer boundary velocities at an inflow condition or the extrapolated velocities at an outflow condition. Additionally, a simple point vortex correction model has been installed to reduce the solution dependency on the size of the outer boundary. Here, circulation on the far-field boundary is set based on the ARC2D computed C_ℓ. Using this velocity correction together with a compressibility correction, modified outer velocities are constructed. It is noted that this correction yields accurate results for domains larger than 4 chords in length (11).

In ZAP2D, a parallel procedure is employed whereby the POT2D computed velocities (currently without compressibility correction) are used as far-field boundary conditions.

3.0 COMPUTED RESULTS

The effectiveness of the coupling procedure installed in ZAP2D is measured by demonstrating accurate and converged solutions for decreasing domain size. In this work, the NACA 0012 airfoil was selected for the validation cases because of the experimental data base (6).

To complete the schedule of computer simulations required in this study, ARC2D and ZAP2D were ported to the Ardent TITAN and also to the IRIS 4D/20G and IRIS 4D/80GT workstations. In addition, graphics routines were also installed on these workstations in order to analyze the results. Furthermore, a new grid generation routine (GRD2D) was written for these machines that can be eventually embedded into ZAP2D and would allow for the possibility of automatic grid manipulation (i.e., grid boundary and density) within ZAP2D iterations.

A total of six grid domains have been utilized to study the blockage effects of the outer boundary on ARC2D and ZAP2D. A description of the grids and their corresponding case identifiers are listed in Table 2. In this table and in the remainder of this report, R_o is normalized by chord length.

GRID	R_o/NO. OF GRID POINTS
A	25/185 X 65
B	12.5/183 X 61
C	5/181 X 57
D	1/177 X 50
E	0.5/177 X 45
F	0.25/177 X 40

Table 2. Grid Cases.

A basic "C" mesh (Figure 9) around the NACA 0012 airfoil was generated by GRD2D which uses an algebraic method where surface normals are maintained. The total number of grid points range from 12,025 (185 x 65) for the largest domain (outer boundary characteristic distance, Ro = 25 chord lengths--Grid A) to 7,080 (177 x 40) for the smallest domain (outer boundary characteristic distance, Ro = 0.25 chord lengths--Grid F). The upper and lower airfoil surface each have 80 grid points for all grids and the wake surface has approximately 13 points. The grid generated is clustered near the surface with a spacing of 2.5×10^{-5} so that at least one point can be embedded within a viscous sublayer. Successive grids were obtained by stripping off outer rings (similar to Ref. 12) to ensure that the spacial distribution over the airfoil remains constant for all grids. Some grid points toward the downstream outflow boundary have also been removed for the smaller grids to reduce the computational domain. Separate studies for the grids used here have proven that this has no effect on the calculations. Finally, the inner and outer boundaries for the smallest grid (F) are illustrated in Figure 9.

Numerical simulations for the NACA 0012 airfoil at two angles of attack are presented here: $\alpha = 4.966°$ and $\alpha = 10°$. For both cases, the Mach number was 0.3 and the Reynolds number was 6 million. Furthermore, the location of the inner boundary coupling surface, S_i, was held fixed (at a distance approximately 10% of the chord from the airfoil) throughout all calculations. Finally, for these calculations, the POT2D simulation was not corrected for Mach number. As the local value of the Mach number at the inner and outer boundaries are quite small, little error should be introduced by this approximation.

3.1 Validation at $\alpha = 4.966°$

Since the inner fluid boundary surface, S_i, is to approximate a potential flow surface, it is logical to validate the coupling concept for an airfoil at low angle of attack and also at low Mach number. Flow separation and transonic effects would only force the inner boundary outward which would possibly diminish some of the improvement in computational effort compared to the simpler problem, but would not invalidate the coupling technique itself. Further, the scheduling (number and frequency) of the potential flow boundary condition updates to the viscous calculation will probably be important as the domain size decreases. This effect should be investigated in detail and is demonstrated in the $\alpha = 10°$ case, but is removed from the current cases illustrated in the following figures by updating only after ARC2D is fully converged. That is, for each domain, a total of 3,000 iterations were utilized with ZAP2D coupling updates every 1,000 iterations.

The effects of domain size (Grids A-F) on the computed integrated forces and moments are compared for ARC2D alone and ZAP2D. The ARC2D simulation is shown for both the point vortex correction (CIRCUL=TRUE) and for no correction (CIRCUL=FALSE). The computational trends of ARC2D for domains smaller than about 4 chords ($1/R_o = 0.25$) are shown here for comparison only since these smaller domains are not recommended practice (11). Finally,

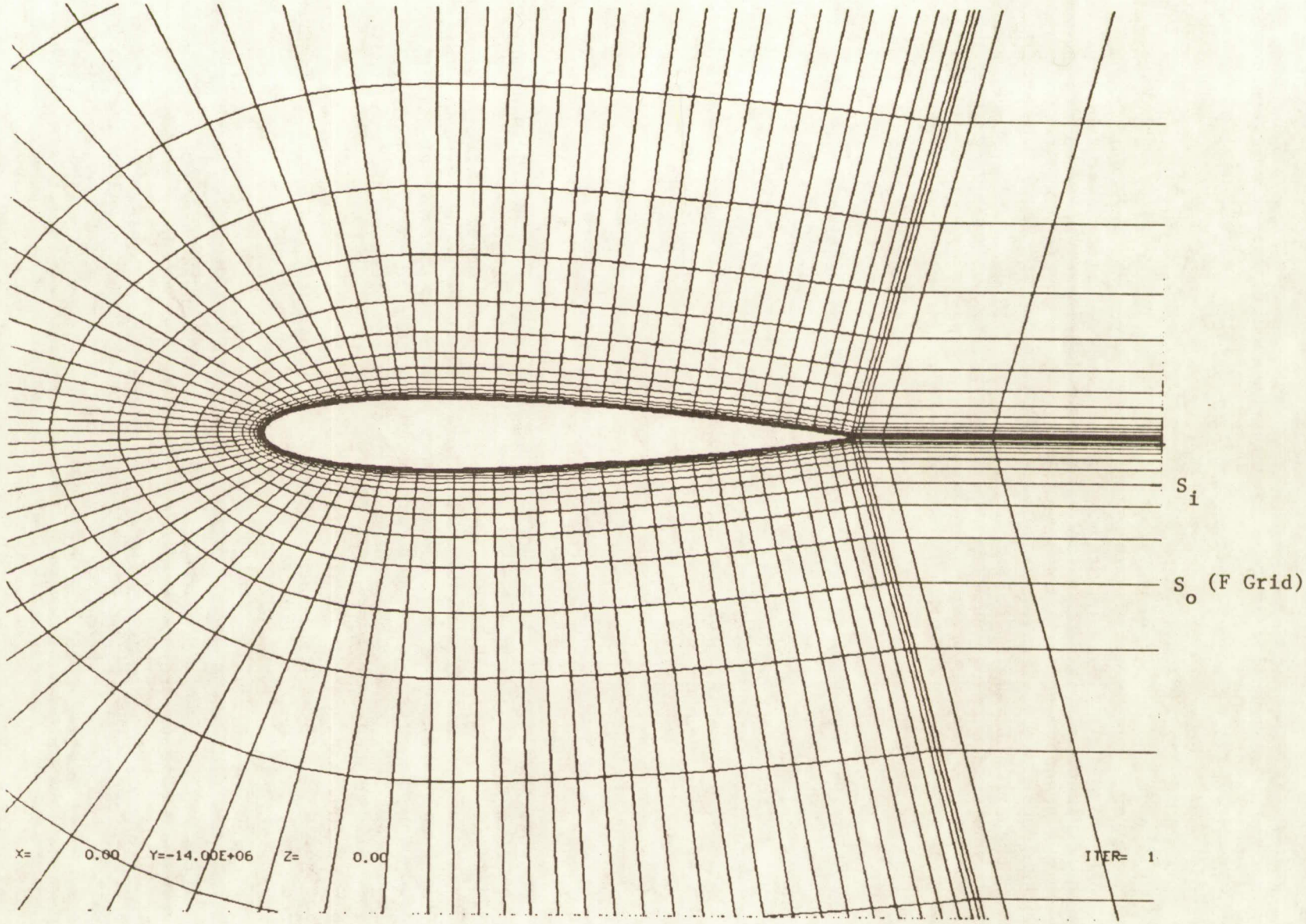

Figure 9. Enlarged View of NACA 0012 Airfoil Grid (185 x 65).

ARC2D calculations are not presented for the smallest grid (F) since the code diverged for this case.

Figure 10 illustrates the effect of domain size on sectional lift coefficient, C_ℓ. Each division represents a change of approximately 2% in C_ℓ compared with the experimental value as shown in the figure. The ZAP2D calculation converges to the ARC2D (CIRCUL=TRUE) solution for $1/R_o$ less than 0.25. Further, for all grids studied, C_ℓ changes from this initial value by less than about 1%, illustrating the utility of the coupled solution in maintaining accuracy for grid domains down to R_o = 1/4 chord. The computed C_ℓ is also within 2% of the experimental value for all grid domains.

Similar results are illustrated in Figures 11 and 12 for sectional drag coefficient, C_d, and sectional pitching moment coefficient about the quarter-chord, C_m, respectively. That is, ZAP2D coupling has removed the effects of domain size on C_ℓ, C_d, and C_m for all grids studied (A-F).

The distribution of surface pressure coefficient, C_p, predicted by ZAP2D for the smallest grid (F) is compared with the experimental values in Figure 13. The correlation is excellent, with viscous effects improving the comparison near the leading and trailing edges over the potential flow case (compare with Figure 5).

Contours of constant Mach number in the flow region near the airfoil are presented in Figure 14. Figure 14(a) illustrates the ARC2D calculation (CIRCUL=FALSE) for the largest domain (A-Grid) while 14(b) illustrates the ZAP2D calculation for the smallest domain (F-Grid). The comparison between the two computed solutions is quite good near the airfoil with a small change in the ZAP2D calculation near the outer boundary of R_o = 0.25.

The numerical stability and convergence characteristics are shown in Figure 15 where the time history of C_ℓ is compared for the first 1,000 iterations for ARC2D (large domain, A-Grid) and ZAP2D (small domain, F-Grid). The increment in the ZAP2D computed C_ℓ for the remaining 2,000 iterations is very small, i.e., for this low angle of attack and this grid size there is very little effect of successive potential flow updates to the outer boundary conditions beyond setting the initial conditions. Still, the ZAP2D time history demonstrates that the coupling procedure is, in fact, a stabilizing influence because it allows for a large reduction of grid domain. As the domain size is reduced, information is passed more quickly throughout the flow field and the oscillatory behavior evident in the ARC2D-alone simulation (Figure 15(a)) is eliminated in the ZAP2D simulation (Figure 15(b)).

Finally, the time histories for the log of the norm of the density residual (Log(Res)) is compared for ARC2D and ZAP2D in Figure 16. The ARC2D large domain, A-Grid calculation is illustrated for the first 1,000 iterations. Further iterations of ARC2D to a maximum of 3,000 does not improve

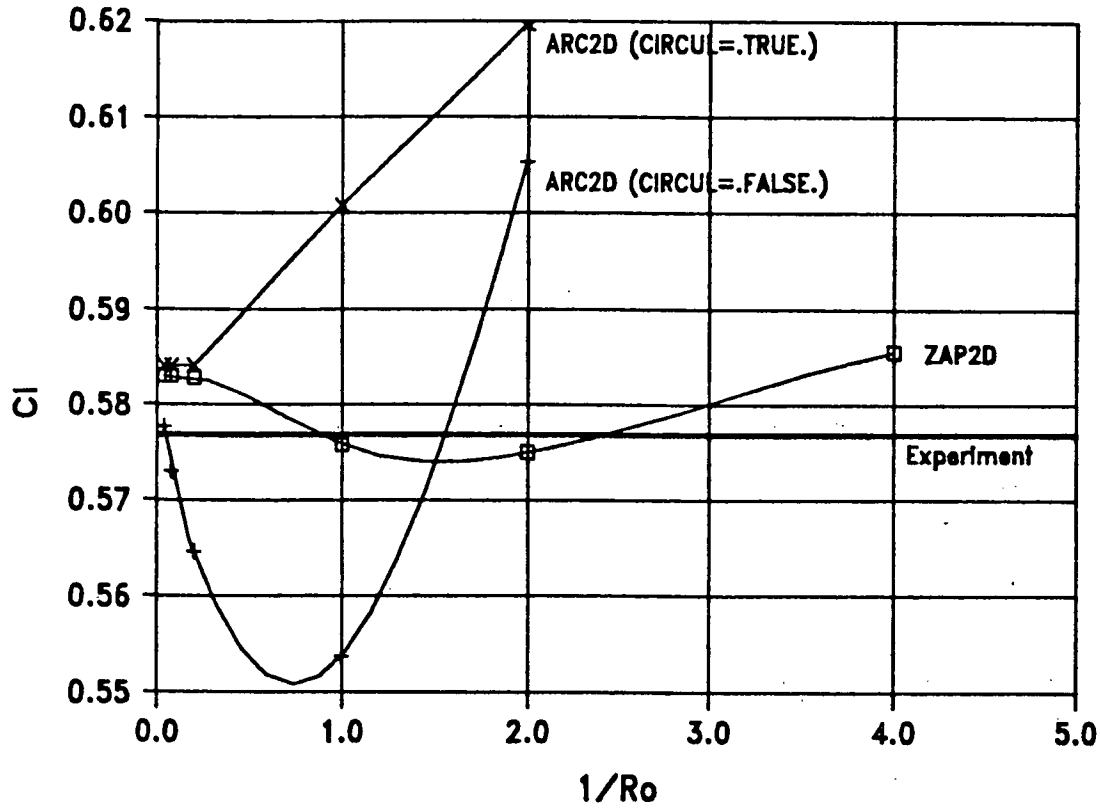

Figure 10. Computed Lift Coefficient Variation with Domain Size for α = 4.966°.

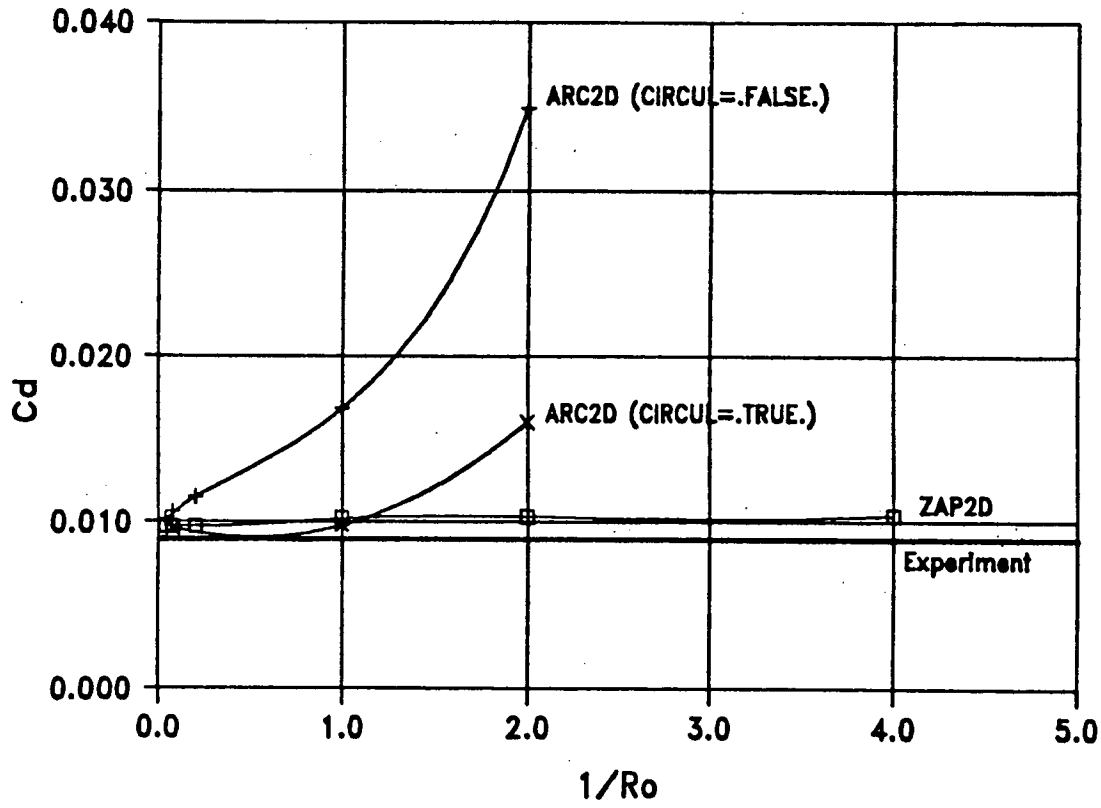

Figure 11. Computed Drag Coefficient Variation with Domain Size for α = 4.966°.

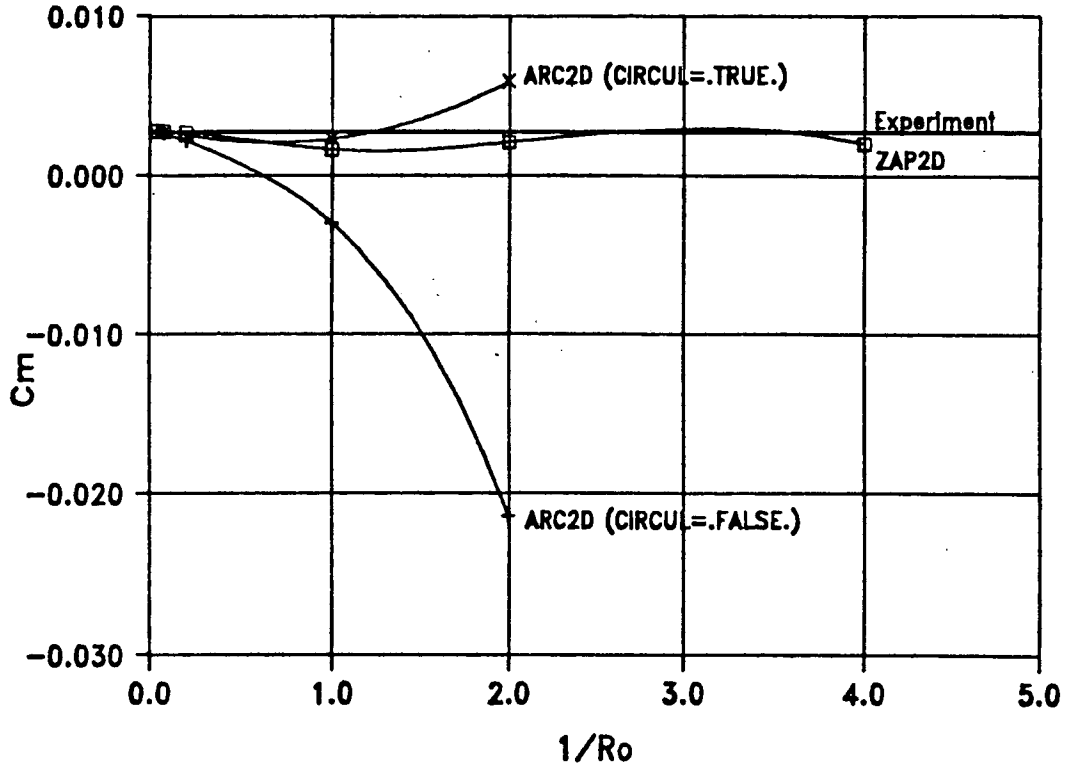

Figure 12. Computed Pitching Moment Coefficient Variation with Domain Size for $\alpha = 4.966°$.

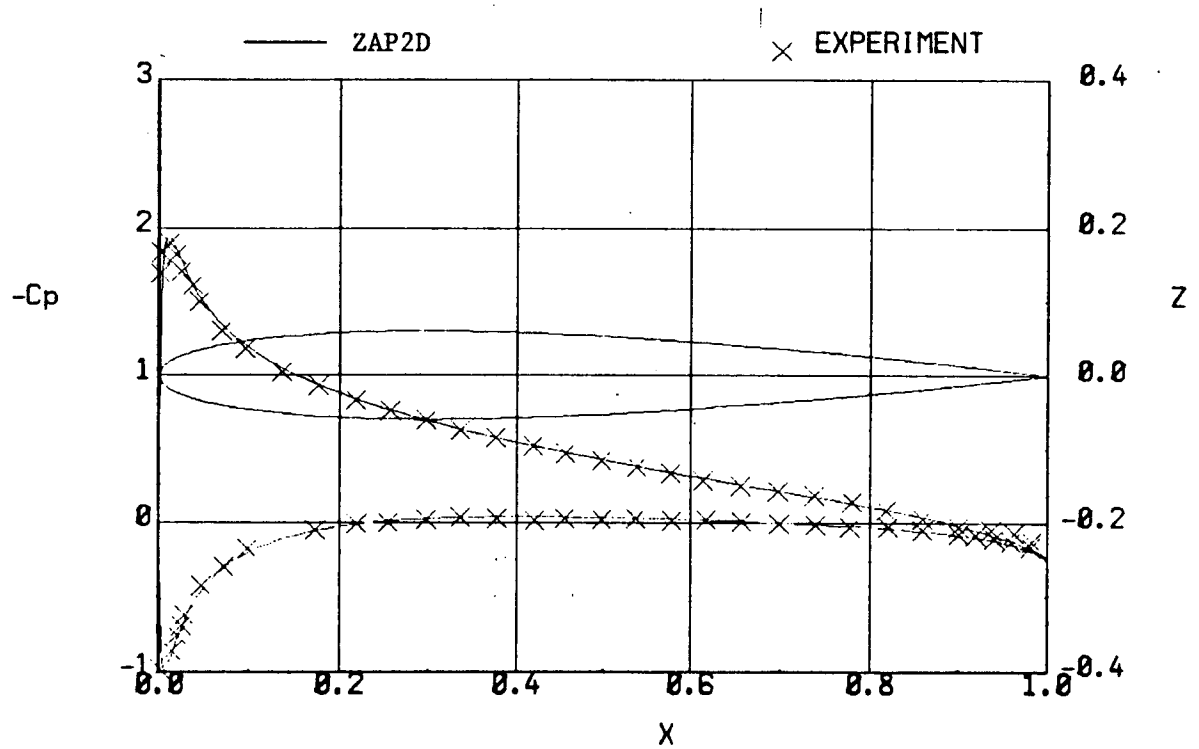

Figure 13. Comparison of ZAP2D (F-Grid) and Experimental Cp Distribution for NACA 0012 Airfoil at Mach 0.3, $\alpha = 4.966°$.

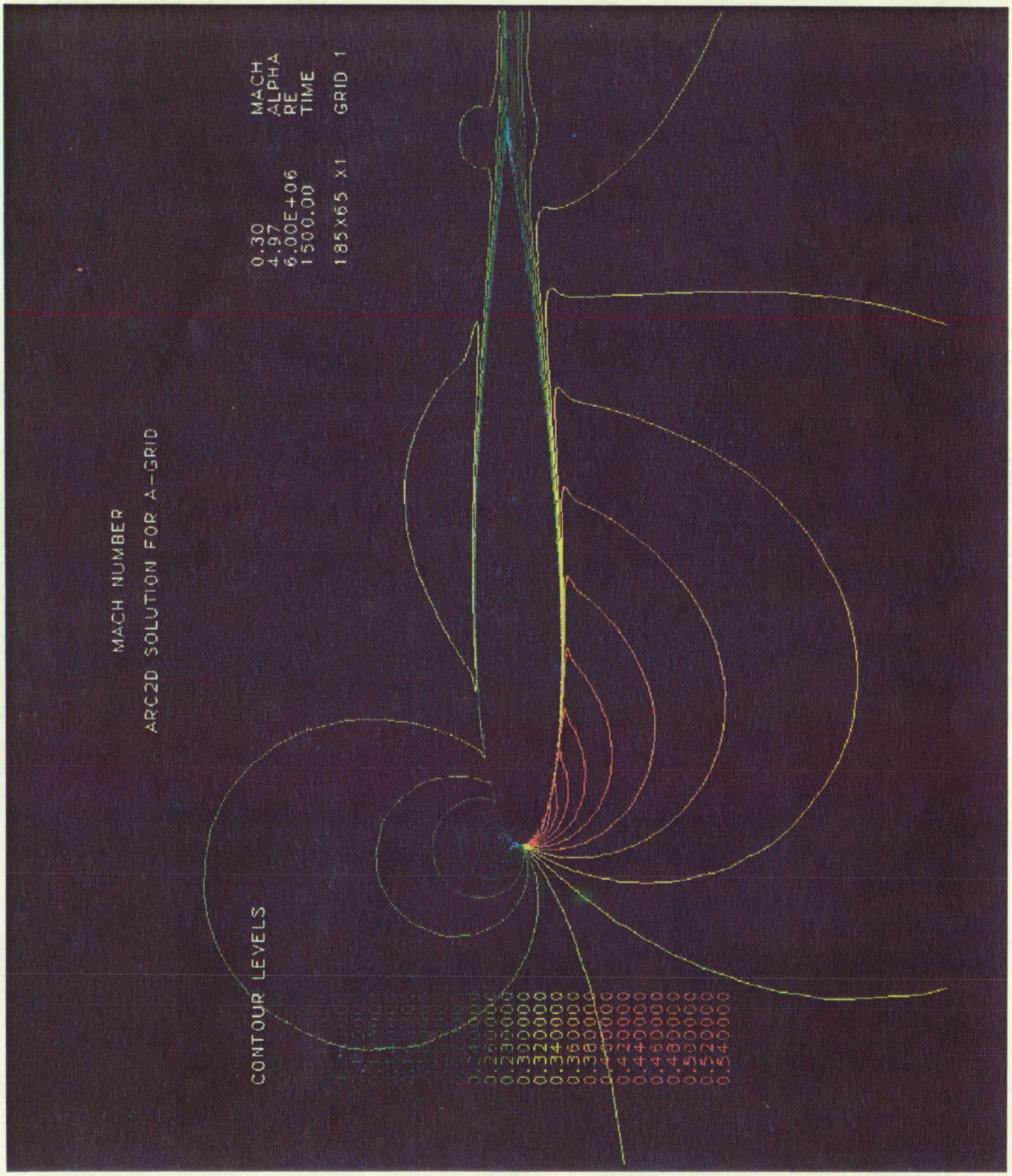

(a) ARC2D with A-Grid (R_o = 25)

Figure 14. Comparison of ZAP2D and ARC2D Computed Mach Contours for NACA 0012 at Mach = 0.3, α = 4.966.

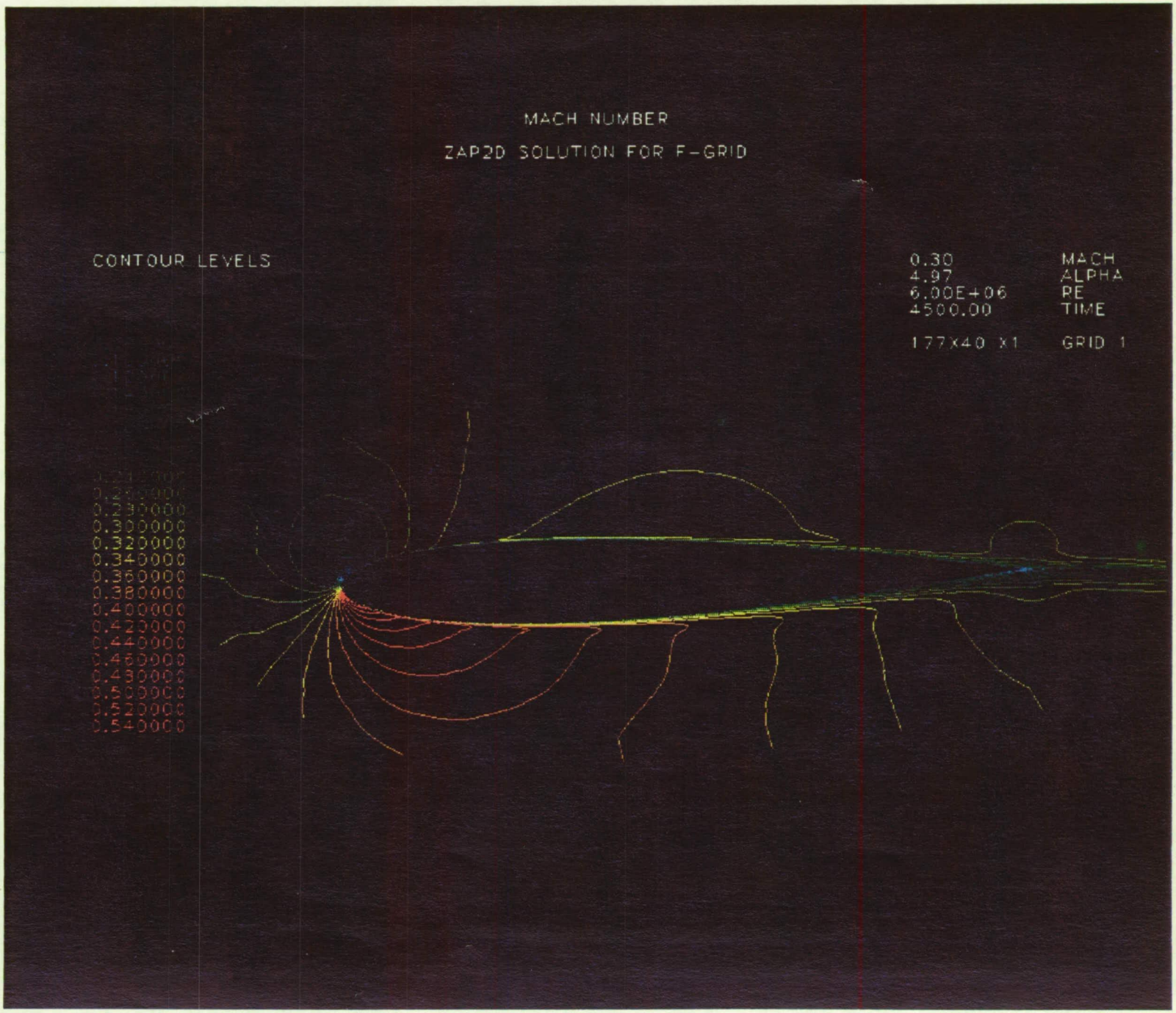

(b) ZAP2D with F-Grid (R_o = 0.25)

Figure 14. Concluded.

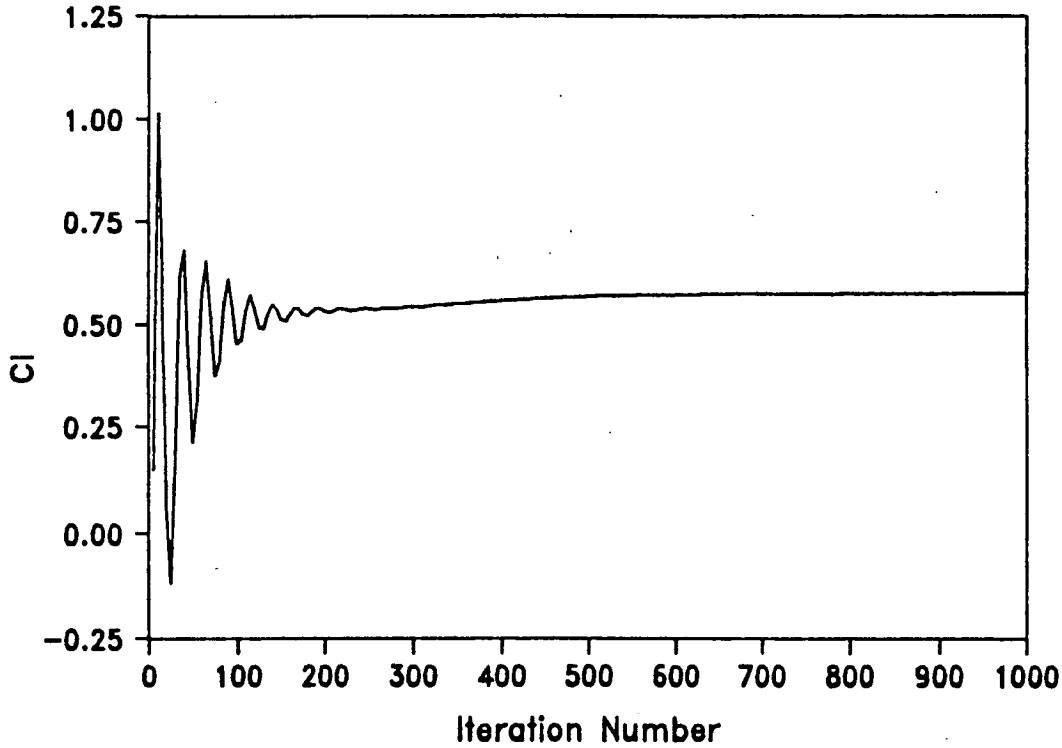

(a) ARC2D with A-Grid (R_o = 25)

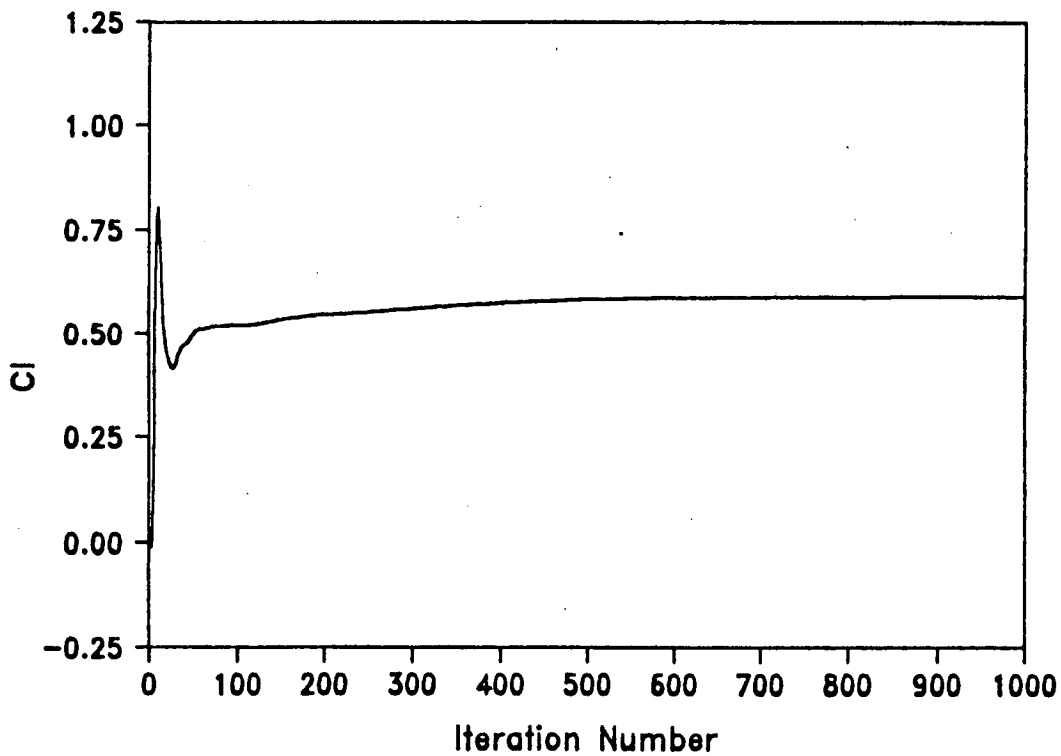

(b) ZAP2D with F-Grid (R_o = 0.25)

Figure 15. Comparison of ZAP2D and ARC2D Computed C_ℓ Iteration History at α = 4.966°, Mach = 0.3.

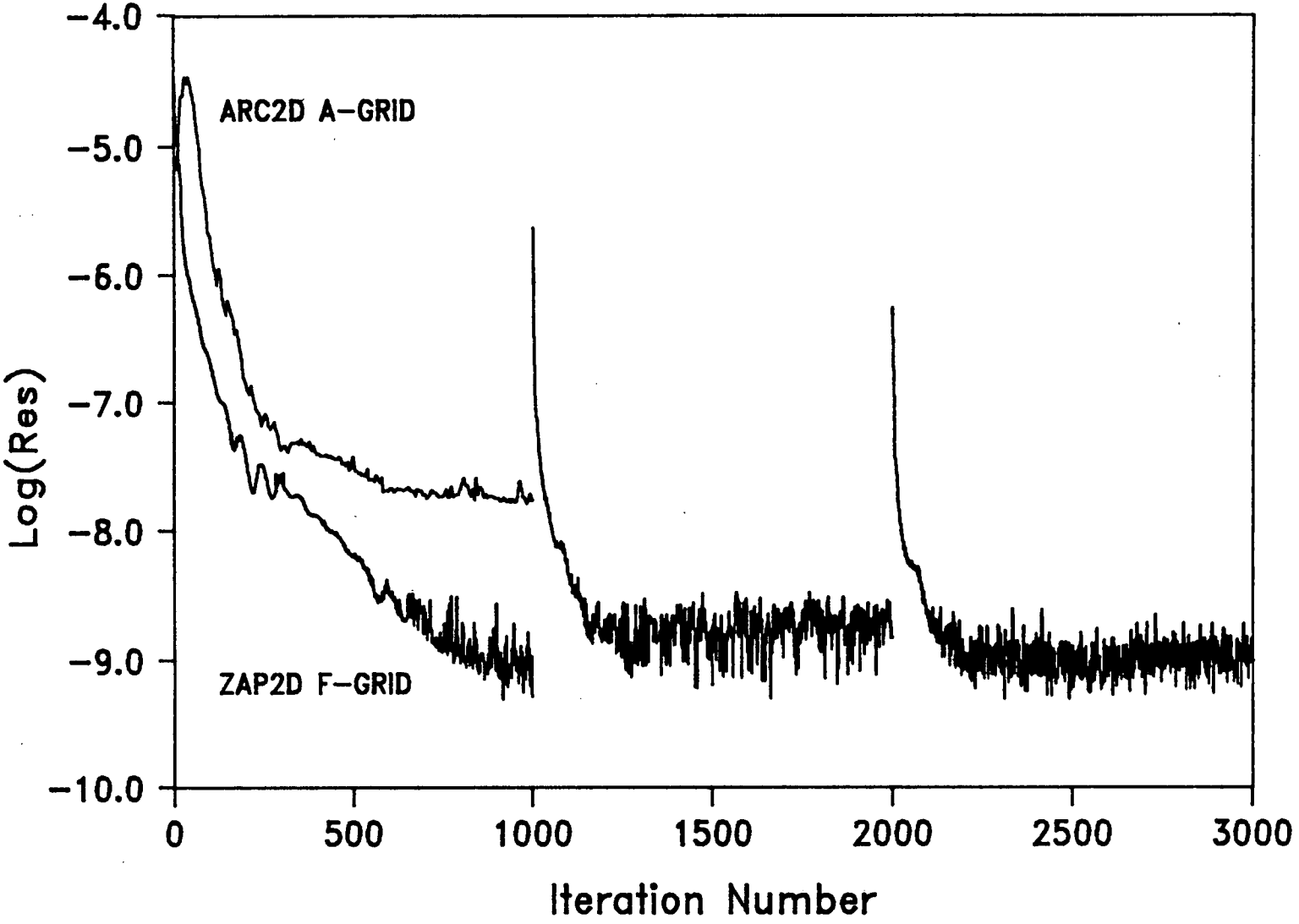

Figure 16. Iteration History of ARC2D and ZAP2D Computed Solution Residual.

convergence from the level indicated at 1,000. The ARC2D simulation shows a reduction in the residue by approximately 3 orders of magnitude. In contrast, the ZAP2D small-domain, F-Grid residual is more rapidly reduced by almost 5 orders of magnitude due to the smaller flow domain. Abrupt changes in the ZAP2D calculation occur due to the outer boundary condition adjustment at the coupled iteration; however, these peaks diminish with further coupled iterations and the solution convergence recovers from each boundary update in less than 100 iterations.

In summary, for the grids utilized in this study of the low angle-of-attack case has shown the following.

1. The coupled procedure installed in ZAP2D allows for a reduction of the outer grid boundary from about 25 chord lengths to 0.25 chord lengths ($R_o = 25 \rightarrow 0.25$) with no loss in accuracy.

2. The numerical convergence of the viscous ARC2D solution is greatly improved due to the reduced domain size allowable in ZAP2D.

3. By utilizing the potential flow solution (ZAP2D) for the initial boundary conditions, a converged solution was obtained for the small domain in contrast to the ARC2D divergent behavior.

4. Multiple potential/viscous boundary condition updates do not significantly affect the final converged solution for the smallest grid studied. This implies that additional grid domain size reduction should be possible without sacrificing accuracy.

5. Without the further improvements in ZAP2D that may be possible such as accelerated convergence methods because of increased stability (Item 2 above) or additional reduction in domain (Item 4), the ZAP2D simulation has still shown a reduction factor of approximately 10 in computer time for a given accuracy and convergence compared with ARC2D alone for this case. This improvement comes from the reduction in grid points and also a reduction of total number of iterations from 1,000 to about 200-300.

3.2 Validation at $\alpha = 10°$

Since the $\alpha = 4.966°$ case did not show that multiple ZAP2D potential/viscous flow updates were required to obtain the needed accuracy for the grids used, the $\alpha = 10°$ case was added to increase the extent of the viscous effects into the flow domain. Because of the limited time for this study, ARC2D was executed with CIRCUL=FALSE only. Furthermore, only Grids D, E, and F were investigated for the ZAP2D calculations since the larger grid cases would certainly converge to the ARC2D-alone results (Section 3.1). Finally, a total number of 1,000 iterations were used for all cases.

As early calculations indicated that intermediate updates would impact the convergence characteristics for this higher angle-of-attack case, a series of ZAP2D update schedules were investigated as outlined in Table 3. For example, the S1 schedule includes the initial POT2D outer boundary conditions only with no intermediate ZAP2D updates while the S6 schedule includes nine intermediate ZAP2D outer boundary updates, 1 after each 100 ARC2D iterations. Schedules S1 through S4 were investigated with Grids D

SCHEDULE	ARC2D ITERATION NUMBER CORRESPONDING TO ZAP2D BOUNDARY UPDATE
S1	1
S2	1, 201
S3	1, 201, 401, 601
S4	1, 201, 401, 601, 801
S5	1, 101, 201, 301
S6	1,. 101, 201, 301, ..., 901

Table 3. Schedule of ZAP2D Outer Boundary Updates.

and E while schedules S5 and S6 were added to the F-Grid cases when the S1 through S4 schedules failed to converge for this small domain. This divergence of ZAP2D for the F-Grid and $\alpha = 10°$ case is in sharp contrast to the same grid and $\alpha = 4.966°$ where intermediate update schedules had very little effect on the solution. Once more, the ARC2D-alone simulation was also divergent for the smallest F-Grid, and the computational trends of the ARC2D-alone simulation for the smaller domains are shown here for comparison purposes only.

The preliminary results for the effect of domain size on the sectional C_ℓ is illustrated in Figure 17. Again, each division represents a change of approximately 2% in C_ℓ compared with the experimental value which is also shown in the figure. The ZAP2D computed C_ℓ for Grids D and E, domain size reduced up to one-half chord ($R_o = 0.5$), and schedule S4 deviates from the experimental C_ℓ and the ARC2D predicted C_ℓ for large domain ($R_o = 25$) by less than 1/2%. The utility of the zonal solution included in ZAP2D in maintaining accuracy with reduced grid domain size is contrasted with the ARC2D-alone solution. On the other hand, while the ZAP2D predictions for Grids D and E are fully converged, the results for the smallest grid, F, are not completed at the present time. For this smallest grid ($R_o = 0.25$), the

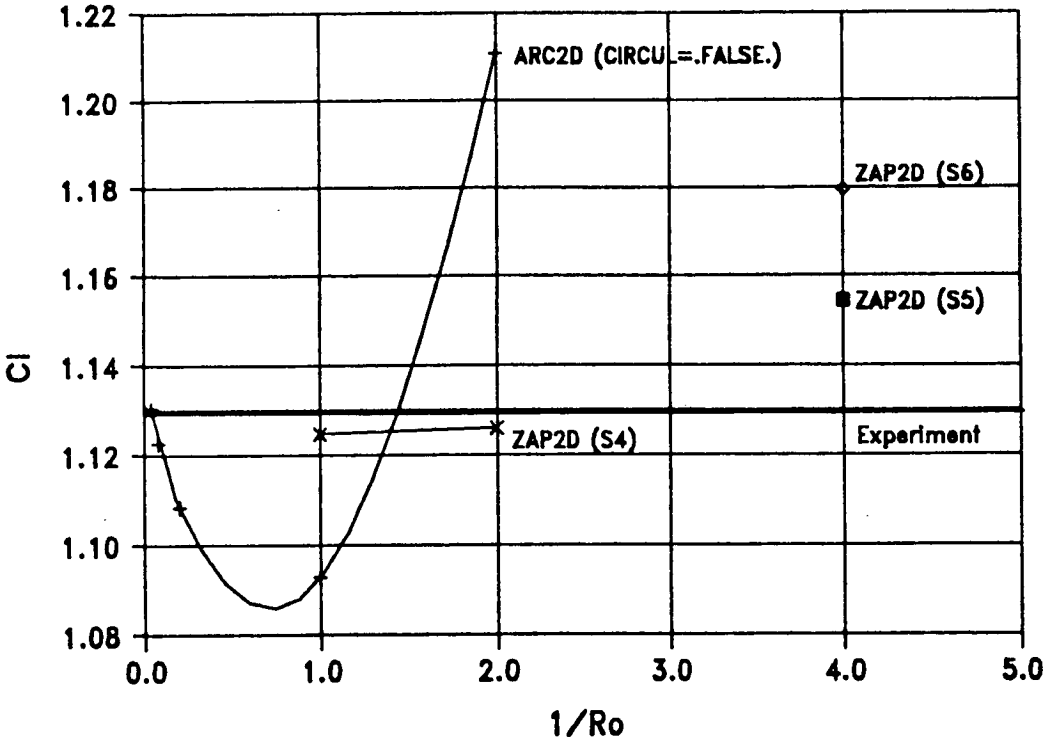

Figure 17. Computed Lift Coefficient Variation with Donain Size for $\alpha = 10°$.

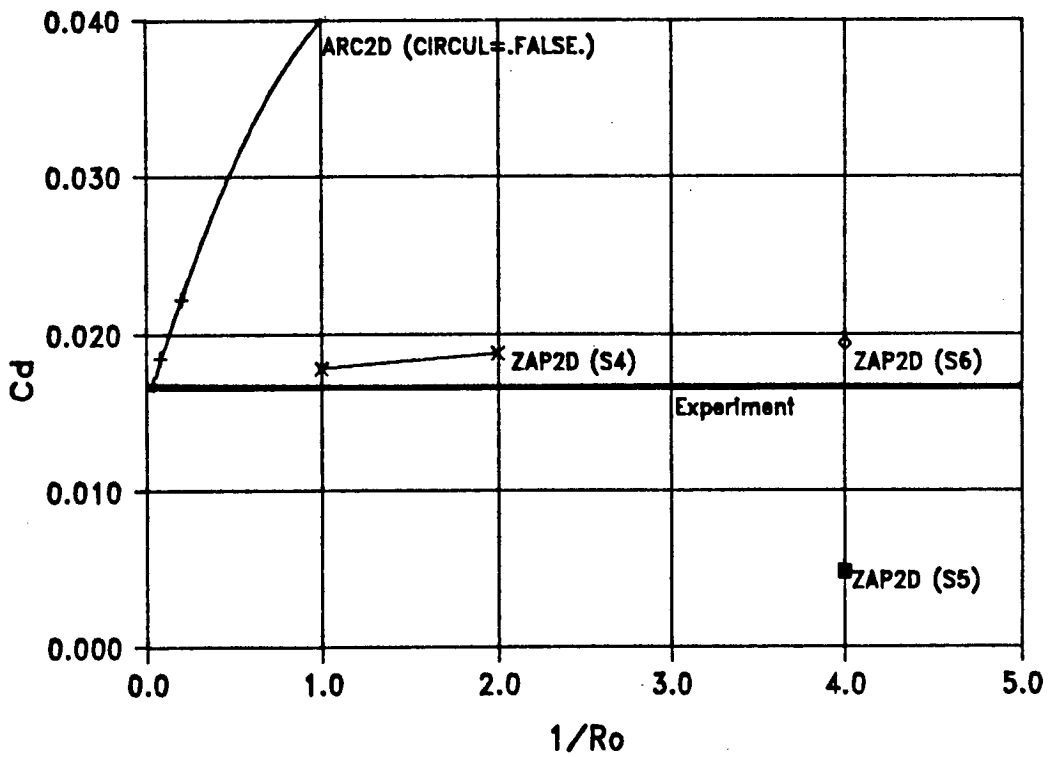

Figure 18. Computed Drag Coefficient Variation with Domain Size for $\alpha = 10°$.

outer boundary update schedule is of extreme importance at this higher angle of attack. As mentioned above, the ZAP2D code diverged for schedules S1 through S4; consequently, schedules S5 and S6 were investigated and ZAP2D solutions for both of these later schedules are shown in Figure 17. In this smaller grid domain, the effects of compressibility or the wake source term (see Section 2.2), which has been neglected in the potential flow updates thus far, may need to be included to obtain a robust ZAP2D solution. An early investigation of this behavior on a Cray computer also indicates that this problem may be related to the Unix installation of ZAP2D on the IRIS and TITAN workstations. Regardless, ZAP2D predicted C_ℓ for the F-Grid for both the S5 and S6 schedules are within approximately 5% of the experimental value.

Similar results for domain dependence are illustrated in Figures 18 and 19 for drag coefficient, C_d, and pitching moment coefficient about the quarter-chord, C_m. The change in the ZAP2D (F-Grid) predicted C_d from the ARC2D (A-Grid) C_d is approximately 10 drag counts and the change in C_m compared with the ARC2D value is approximately 0.001 for grid domain reductions to one-half chord. On the other hand, the pitching moment predictions for both ARC2D and ZAP2D are approximately $C_m = 0.01$ while the experimental value is almost double this level. While no explanation is given for the difference at this time, it does illustrate that the zonal coupling in ZAP2D cannot improve upon a fully converged, large domain, ARC2D solution.

The ZAP2D predicted distribution of surface pressure coefficient, C_p, for $\alpha = 10°$ and the E-Grid is compared with experimental measurements for corrected $\alpha_c = 10.122°$ in Figure 20. The data correlation is excellent over the entire airfoil with a small underprediction of the leading-edge suction peak. This error is most likely a result of the slightly lower angle of attack used in the numerical simulation. A similar comparison of the pressure distribution (not shown here) for the F-Grid indicates that the pressure distribution is converged except near the leading-edge suction peak where $C_{p_{min}}$ (S5) = -6.25 and $C_{p_{min}}$ (S6) = -6.38.

A final set of three figures are included here to demonstrate the effect of intermediate outer boundary updates (i.e., in this case, updates before a fully converged ARC2D solution) on the ZAP2D-E-Grid iteration history. Figures 21 and 22 illustrate the ZAP2D solution iteration history for C_ℓ and C_d for intermediate update schedules S1 through S4. Since the S1 schedule includes only the initial outer boundary potential flow correction, the impact of the various intermediate outer boundary update schedules (S2-S4) is evident in Figures 21 and 22. As shown, the amplitude of the C_ℓ and C_d increments at the scheduled outer boundary update periods decreases during the time-step iteration history. Finally, the convergence of the integrated forces and moment for this case as a function of number of intermediate outer boundary updates is shown in Figure 23. For all coefficients, C_ℓ, C_d, and C_m, convergence is clearly demonstrated. The percentage change in

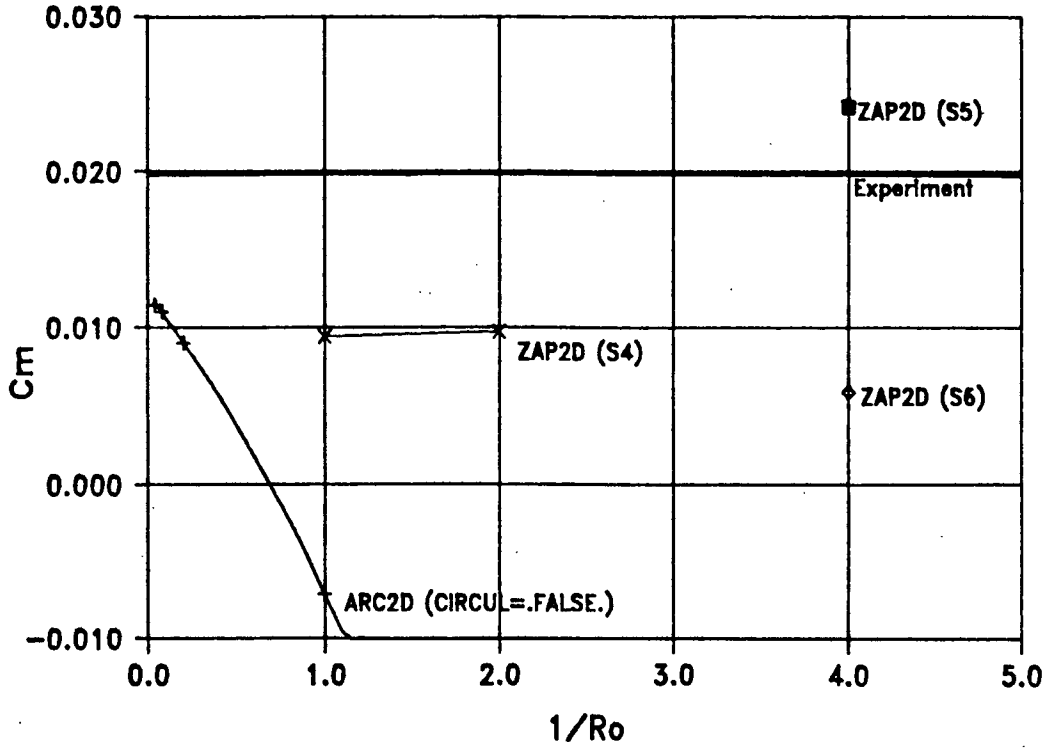

Figure 19. Computed Pitching Moment Coefficient Variation with Domain Size for $\alpha = 10°$.

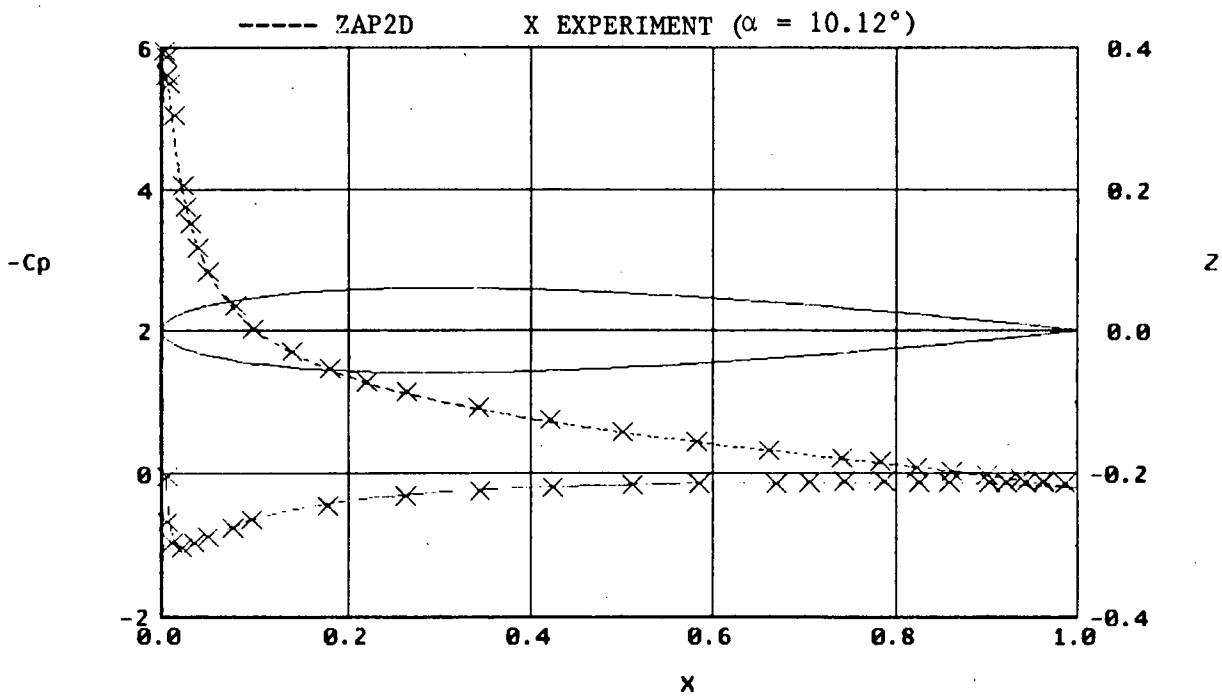

Figure 20. Comparison of ZAP2D (E-Grid) and Experimental Cp Distribution for Mach = 0.3, $\alpha = 10°$.

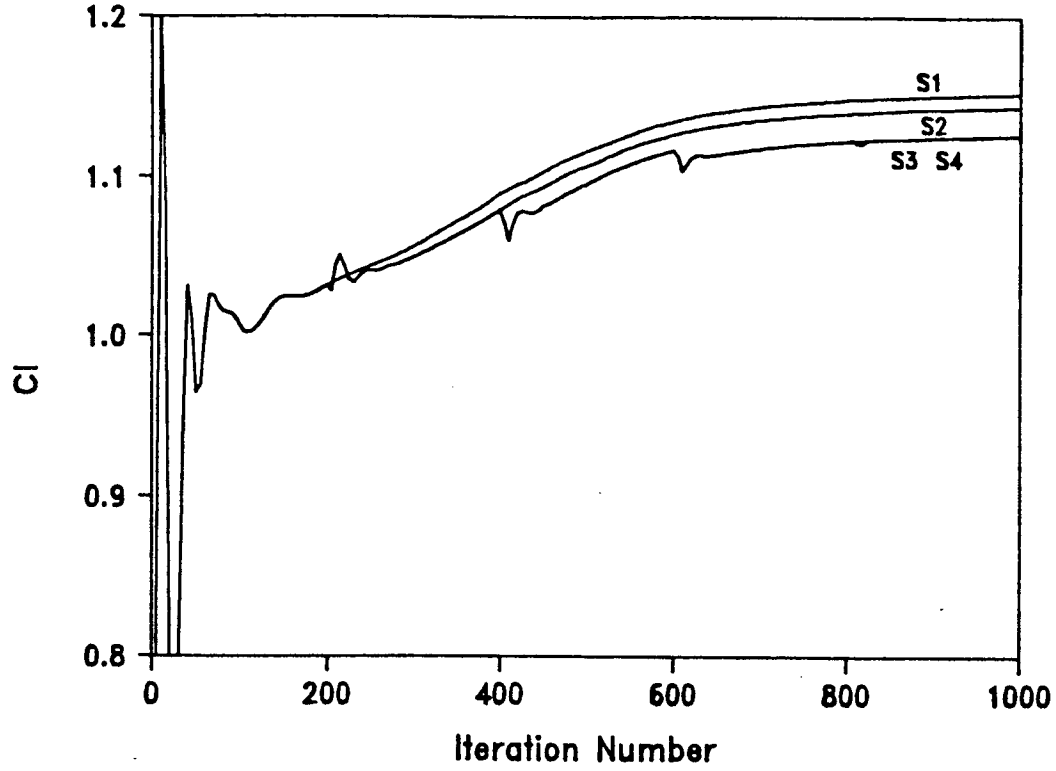

Figure 21. Iteration History of ZAP2D (E-Grid) Calculated C_ℓ (Mach = 0.3, α = 10°) for Various Outer Boundary Update Schedules.

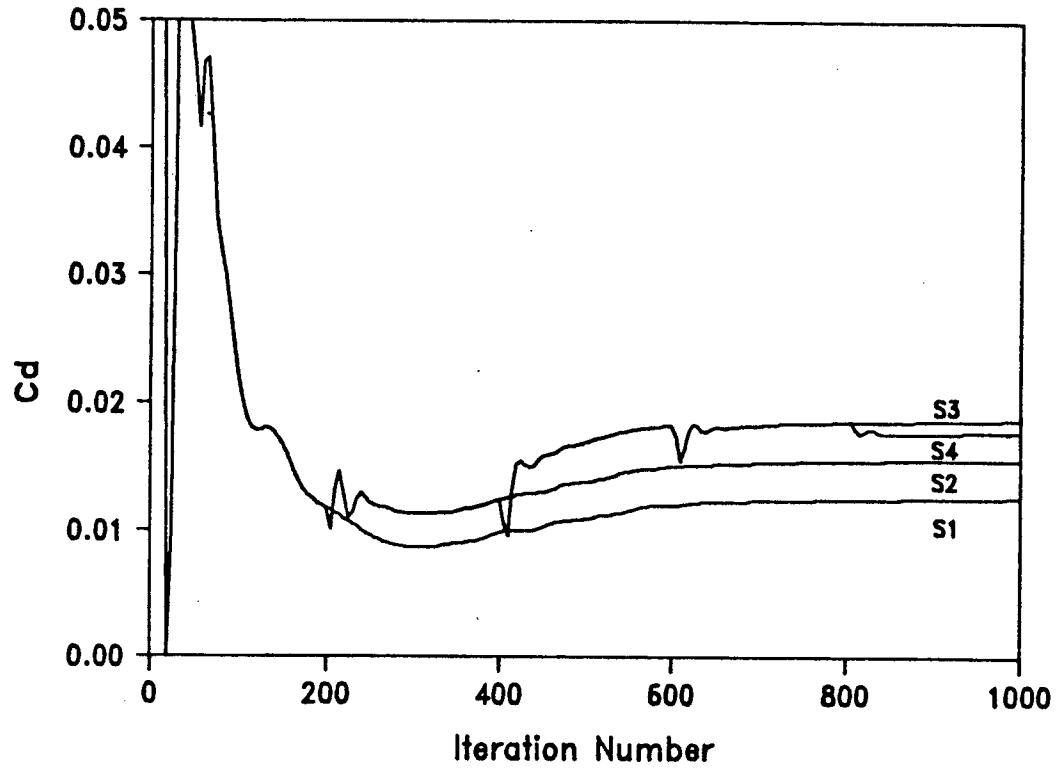

Figure 22. Iteration History of ZAP2D (E-Grid) Calculated C_d (Mach = 0.3, α = 10°) for Various Outer Boundary Update Schedules.

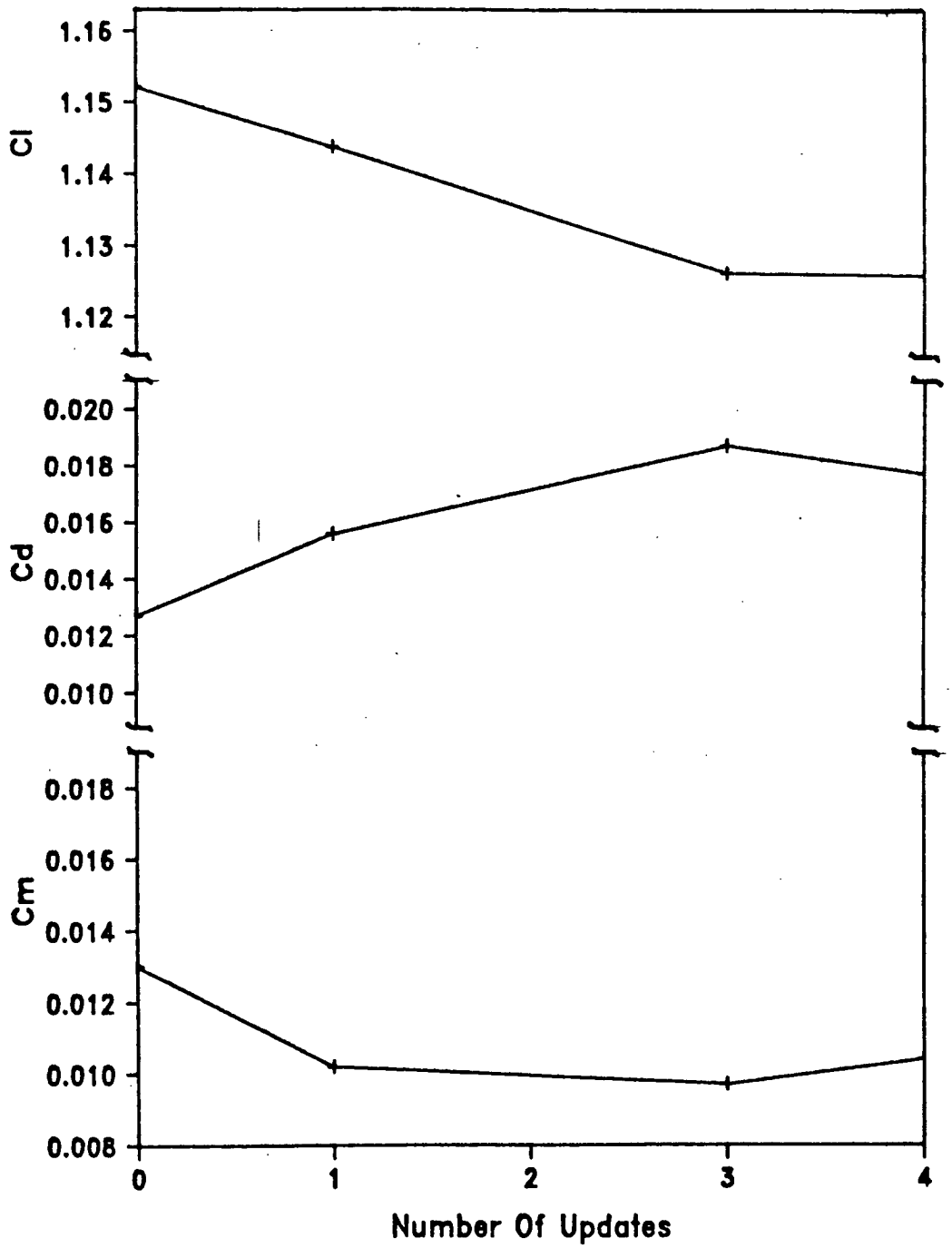

Figure 23. ZAP2D Force and Moment Convergence Trend for E Grid as a Function of Outer Boundary Update Schedule (Mach = 0.3, α = 10°).

the coefficients from their initial (S1 schedule) to their final (S4 schedule) values is as follows.

$$\% \Delta C_{\ell} \approx 2\ 1/4\%$$

$$\% \Delta C_{d} \approx 40\%$$

$$\% \Delta C_{m} \approx 20\%$$

Consequently, while the percentage change in C_{ℓ} is small, the change in C_{d} and C_{m} are quite significant.

In summary, this abbreviated study of the high angle-of-attack case has shown the following additional features.

1. The coupled procedure installed in ZAP2D allows for a reduction of the outer grid boundary from 25 chord lengths to 0.5 chord lengths with no loss in accuracy.

2. While the smallest grid, F, has not been resolved to the same accuracy level at this time, it has been demonstrated that additional outer boundary schedule updates in ZAP2D will most likely yield converged results within the required accuracy. Undoubtedly, the compressibility correction will also need to be added to ZAP2D for this case.

3. Multiple ZAP2D potential/viscous outer boundary condition updates do affect the final converged solution and are required to obtain an accurate solution for all forces and moments.

4. As the grid domain is decreased, the schedule of ZAP2D intermediate outer boundary updates directly affects the robustness of the ARC2D solution scheme (all other parameters fixed) in that a solution can be obtained where it was previously divergent.

4.0 CONCLUSIONS

The primary objective of the work described in this report is to demonstrate the feasibility of a new potential/viscous coupling procedure for reducing computational effort while maintaining solution accuracy. The overlapping velocity coupling procedure has been used to combine a two-dimensional potential flow code, POT2D, and a two-dimensional Navier-Stokes code, ARC2D.

The resultant fully coupled code, ZAP2D, was utilized to compute the flow past a NACA 0012 airfoil at 4.966° and 10° angle of attack. The Mach number was 0.3 and the Reynolds number was 6 million for both cases. A thorough study of the numerical behavior of the computed solutions for a range of grid domain sizes from 25 chord lengths to 0.25 chord lengths and comparison with experimental data has demonstrated the following.

1. The coupled procedure installed in ZAP2D allows for a reduction of the outer grid boundary from about 25 chord lengths to 0.25 chord lengths with no loss in accuracy.

2. The numerical convergence of the viscous ARC2D solution is greatly improved due to the reduced domain size allowable in ZAP2D.

3. The zonal modeling in ZAP2D increases the robustness of the ARC2D solution scheme in that numerical divergence of ARC2D-alone is avoided for the smallest domain.

4. As the Navier-Stokes computational domain is decreased and viscous (or Mach number) effects become more important, multiple ZAP2D potential/viscous outer boundary condition updates are required to obtain accurate and converged solutions.

5. For the $\alpha = 4.96°$ case, the ZAP2D simulation has demonstrated a reduction factor of approximately 10 in computer time for given accuracy and convergence compared with the ARC2D-alone simulation. With some additional effort, the $\alpha = 10°$ case should also show similar improvements.

It is expected that by investigating additional reductions in domain size, the use of accelerated convergence methods because of the increased computational stability (Item 2 above), and optimization of AZP2D update schedules (Item 4 above), the computational time for the two-dimensional ZAP2D simulation might be reduced by a factor of approximately 20 when compared with the ARC2D simulation. If similar grid density reductions are possible in three dimensions, then the required grid for a given accuracy might be reduced by about 70%; i.e., only 25-30% of the large domain grid would be required for a fully coupled, three-dimensional solution. This would translate into a significant reduction in memory requirements corresponding to the reduction in number of grid points. Furthermore, additional improvements in the convergence behavior due to the smaller domain would also be possible so that perhaps one-half the number of iteration steps would be required with such a zonal method. Of course, additional overhead in computing the potential flow updates would be incurred in the three-dimensional simulation; however, a conservative estimate of at least one

order of magnitude reduction in computational time compared with the Navier-Stokes-only method should be achievable for a given accuracy in such a zonal simulation. This improvement would allow for a much more accurate three-dimensional simulation of the complex flow fields associated with rotary wing aircraft.

5.0 REFERENCES

1. Pulliam, T.H., and Steger, J.L., "Implicit Finite Difference Simulations of Three-Dimensional Compressible Flow", AIAA Paper 78-10, 1978.

2. Maskew, B., "Prediction of Subsonic Aerodynamic Characteristics: A Case For Low-Order Panel Methods", J. Aircraft, Vol. 19, No. 2, February 1982.

3. Lamb, H., Hydrodynamics, 6th Edition, Dover Publications, New York, 1945.

4. Morino, L., "Unsteady Compressible Potential Flow around Lifting Bodies Having Arbitrary Shapes and Motions", TR-72-01, Boston University, June 1972.

5. Shapiro, A.H., The Dynamics and Thermodynamics of Compressible Fluid Flow, Volume I, The Ronald Press Co., New York, 1953.

6. Harris, C.D., "Two-Dimensional Aerodynamic Characteristics of the NACA 0012 Airfoil in the Langley 8-Foot Transonic Pressure Tunnel", NASA TM-81927, April 1981.

7. Pulliam, T.H., Jespersen, D.C., and Childs, R.E., "An Enhanced Version of an Implicit Code for the Euler Equations", AIAA-83-0344, 1983.

8. Pulliam, T.H., and Steger, J.L., "Recent Improvements in Efficiency, Accuracy, and Convergence for Implicit Approximate Factorization Algorithms", AIAA 85-0360, 1985.

9. Pulliam, T.H., "Efficient Solution Methods for the Navier-Stokes Equations", Lecture Note for the von Karman Institute for Fluid Dynamics Lecture Series: Numerical Techniques for Viscous Flow Computation in Turbomachinery Bladings, von Karman Institute, Rhode-St.-Genese, Belgium, 1985.

10. Baldwin, B.S., and Lomax, H., "Thin Layer Approximation and Algebraic Model for Separated Turbulent Flows", AIAA-78-257, 1978.

11. Maksymiuk, C.M. and Pulliam, T.H., "Viscous Transonic Airfoil Workshop Results using ARC2D", AIAA-87-0415, 1987.

NASA
National Aeronautics and Space Administration

Report Documentation Page

1. Report No.	2. Government Accession No.	3. Recipient's Catalog No.
NASA CR-177568		

4. Title and Subtitle	5. Report Date
A Novel Potential/Viscous Flow Coupling Technique for Computing Helicopter Flow Fields	August 1990
	6. Performing Organization Code

7. Author(s)	8. Performing Organization Report No.
J. Michael Summa, Daniel J. Strash, and Sungyul Yoo	A-90283
	10. Work Unit No. 505-61-51

9. Performing Organization Name and Address	11. Contract or Grant No.
Analytical Methods, Inc. 2133 152nd Avenue N.E. Redmond, WA 98052	NAS2-12962
	13. Type of Report and Period Covered Contractor Report
12. Sponsoring Agency Name and Address National Aeronautics and Space Administration Washington, DC 20546-0001	14. Sponsoring Agency Code

15. Supplementary Notes

Point of Contact: Paul Stremel, Ames Research Center, MS T-042, Moffett Field, CA 94035-1000
(415) 604-4563 or FTS 464-4563

16. Abstract

Because of the complexity of the helicopter flow field, a zonal method of analysis of computational aerodynamics is required. In this research, a new procedure for coupling potential and viscous flow calculation schemes is proposed. An overlapping, velocity-coupling technique is to be developed with the unique feature that the potential flow surface singularity strengths are obtained directly from the Navier-Stokes solution at a smoother inner fluid boundary. The closed-loop iteration method proceeds until the velocity field is converged. This coupling should provide the means of more accurate viscous computations of the near-body and rotor flow fields with resultant improved analysis of such important performance parameters as helicopter fuselage drag and rotor airloads.

17. Key Words (Suggested by Author(s))	18. Distribution Statement
Potential flow Viscous flow Zonal modeling/Helicopter aerodynamics	Unclassified–Unlimited Subject Category–02

19. Security Classif. (of this report)	20. Security Classif. (of this page)	21. No. of Pages	22. Price
Unclassified	Unclassified	44	A03

NASA FORM 1626 OCT 86

For sale by the National Technical Information Service, Springfield, Virginia 22161